Lithos 320–321 (2018) 280–301

Contents lists available at ScienceDirect

Lithos

journal homepage: www.elsevier.com/locate/lithos

Age and chemical composition of Archean metapelites in the Zhongxiang Complex and implications for early crustal evolution of the Yangtze Craton

Kai Wang [a,b,c], Shuwen Dong [d,e,*], Zheng-Xiang Li [c], Baofu Han [b]

[a] Chinese Academy of Geological Sciences, Beijing 100037, China
[b] Ministry of Education Key Laboratory of Orogenic Belts and Crustal Evolution, School of Earth and Space Sciences, Peking University, Beijing 100871, China
[c] Earth Dynamics Research Group, The Institute for Geoscience Research (TIGeR) and ARC Centre of Excellence for Core to Crust Fluid Systems (CCFS), School of Earth and Planetary Sciences, Curtin University, Perth, WA 6845, Australia
[d] School of Earth Sciences and Engineering, Nanjing University, Nanjing 210093, China
[e] SinoProbe Center, Chinese Academy of Geological Sciences, Beijing 100037, China

ARTICLE INFO

Article history:
Received 6 June 2018
Accepted 22 September 2018
Available online 27 September 2018

Keywords:
Chemical composition
Metapelites
Yangpo "Group"
Zhongxiang Complex
Yangtze Craton
Archean continental crust

ABSTRACT

Chemical composition of sedimentary rocks bears important clues on source rock characteristics and sedimentary processes, providing a critical record of the evolving continental crust. Whole-rock major and trace elements, and detrital zircon U-Pb-Hf isotopic data for metapelites of the Archean Yangpo "Group" in the newly discovered Zhongxiang Complex, South China, are employed to investigate the age, provenance, and sedimentary processes of the protoliths, so as to further characterize the early crustal evolution of the Yangtze Craton. Detrital zircon cores from the metapelites yielded a youngest age of around 2.70 Ga with metamorphic rims dated at 1.95 Ga, which in combination with previous geochronological studies on granitic bodies intruding the Yangpo "Group" constrain the depositional age between 2.70 and 2.67 Ga. This makes the protolith of the Yangpo "Group" the oldest sedimentary unit in the Yangtze Craton. Geochemical signatures of the metapelites indicate relatively weak chemical weathering of the source area and weak to moderate post-depositional silicification and K-metasomatism. Diagnostic trace element ratios and REE patterns suggest that the protoliths of the Yangpo metapelites are compositionally immature with a mixed source of (ultra)-mafic (>60%) and felsic rocks, which possibly accumulated in a basin near an active continental margin. Detrital zircons in the Yangpo metapelites are dominated by 2.92–2.85 Ga and 2.80–2.73 Ga age populations with two prominent peaks at 2.87 Ga and 2.78 Ga, which are in agreement with the zircon ages and Hf isotopic compositions of the known older magmatic rocks in the Zhongxiang Complex, indicating that the proximal basement rocks were the principal detrital source. Integrated zircon age and Hf-isotope data suggest that the Archean continental crust of the Zhongxiang Complex was built through three major episodes of crustal growth at 3.55–3.45 Ga, 3.40–3.0 Ga, and 2.92–2.85 Ga, followed by two major episodes of crustal reworking at 2.80–2.70 Ga and 2.67–2.62 Ga. Such a crustal history distinguishes the Zhongxiang Complex from other Archean crustal provinces of the Yangtze Craton, pointing to a complex Archean evolutionary history for the Yangtze Craton.

1. Introduction

The Archean Eon features the early generation of continental crust from the mantle. Knowledge of the chemical composition of the Archean continental crust is therefore fundamental for understanding the early evolution of our planet (Halla et al., 2017; Taylor and McLennan, 1985). Whereas partial melting of basaltic rocks from either subducted oceanic crust (e.g.,Martin et al., 2014; Polat, 2012) or thickened, plateau-like mafic crust (e.g.,Johnson et al., 2017; Nageletal., 2012) that led to the emplacement of TTGs (tonalite-trondhjemite-granodiorite) is a well-established process for the generation of Archean continents, sedimentary record that tracks early continental erosion and surface environments has been rare (e.g.,Bolhar et al., 2005, 2015; Garçon et al., 2017; Wang et al., 2012a, 2016a, 2017). Instead of TTGs that dominate the preserved Archean provinces worldwide, greenstones including metasedimentary rocks which have largely been eroded are commonly believed to have been the major component of the Archean continental crust (Condie, 1993; McLennan and Taylor, 1991; Taylor and McLennan, 1985). Archean sedimentary rocks are often regarded as an ideal archive for eroded crustal materials

* Corresponding author at: Department of Earth Sciences, Nanjing University, 163 Xianlin Road, School of Earth Sciences and Engineering, Nanjing 210093, PRChina.
E-mail address: swdong@nju.edu.cn (S. Dong).

https://doi.org/10.1016/j.lithos.2018.09.027
0024-4937/

which may no longer be present at the surface, making them good targets for exploring the nature and genesis of the Archean upper continental crust (Condie, 1993; Gao et al., 1999; McLennan et al., 1993; Taylor and McLennan, 1985). Therefore, characterizing the chemical composition of Archean sedimentary rocks and their likely provenances is crucial for understanding the early generation and evolution of the continental crust.

In the Yangtze Craton, South China, Archean rocks are only documented in several spatially restricted crustal provinces along the craton margins, and they consist mainly of TTG gneisses and other granitic rocks that have been studied in terms of geochronology and geochemistry (Fig. 1; Table 1; e.g.,Guo et al., 2015; Hui et al., 2017; Wang et al., 2018). Some Archean-Paleoproterozoic metasedimentary rocks have also been recognized from the Kongling, Yudongzi, and Zhongxiang complexes in the northern Yangtze Craton, the Tangdan Group and the Dongchuan Group (and its equivalents the Dahongshan and Hekou groups) in the southwestern Yangtze Craton, as well as within the Huangtuling granulites in the Dabie region, which contain significant information on the early crustal processes. However, the age and chemical composition of these metasedimentary rocks are largely unclear (Fig. 1b; e.g.,Wu et al., 2008; Wang et al., 2013a; Yin et al., 2013; Wang and Zhou, 2014; Li et al., 2016), thus hampering a better understanding of the Archean evolutionary history of the Yangtze Craton.

Metasedimentary rocks of the newly discovered Zhongxiang Complex, termed the Yangpo "Group" (BGMRHP, 1990; HIGS, 1965), represent an ancient sedimentary record of the Yangtze Craton. It has recently been suggested that quartz schists of the Yangpo "Group" may have been deposited in the Neoarchean (Wang et al., 2013a), but the precise timings of deposition and metamorphism, and the primary chemical composition of the Yangpo "Group" sediments are not well constrained, and their provenance and sedimentary environment are equivocal. We report in this study metapelites of the Yangpo "Group" and focus on these fine-grained sediments as they usually possess higher abundances of immobile elements than sandstones, such as REE (Rare Earth Elements), Th, and Sc, and can be more useful indicators of the upper continental crustal composition (Condie, 1993; Ghosh and Sarkar, 2010; Young, 1999). We carried out systematic detrital zircon U-Pb-Hf isotopic and whole-rock geochemical analyses on the Yangpo metapelites in order to (i)constrain the timing of deposition and/or thermal overprinting, (ii) characterize the nature of source materials and investigate the provenance of the Yangpo metapelites, (iii) discern possible depositional setting, and (iv) provide constraints on the Archean continental crustal evolution of the Yangtze Craton.

2. Geological setting

2.1. Regional geology

The Precambrian rocks of South China is generally divided into two different crustal elements: the Yangtze Craton (or Block) to the northwest and the Cathaysia Block to the southeast, which were welded together along the Neoproterozoic Sibao (Jiangnan) orogenic belt (Fig. 1; e.g.,Chen et al., 1991; Li et al., 1995, 2002; Zhao and Cawood, 2012). The Yangtze Craton, including sections of the Sibao orogenic belt, features a prolonged Precambrian evolutionary history from Paleoarchean to Neoproterozoic (Fig. 1b). Late Mesoproterozoic to Neoproterozoic weakly metamorphosed volcanic-sedimentary successions and plutonic rocks dominate the Precambrian outcrops, with rare Archean to early

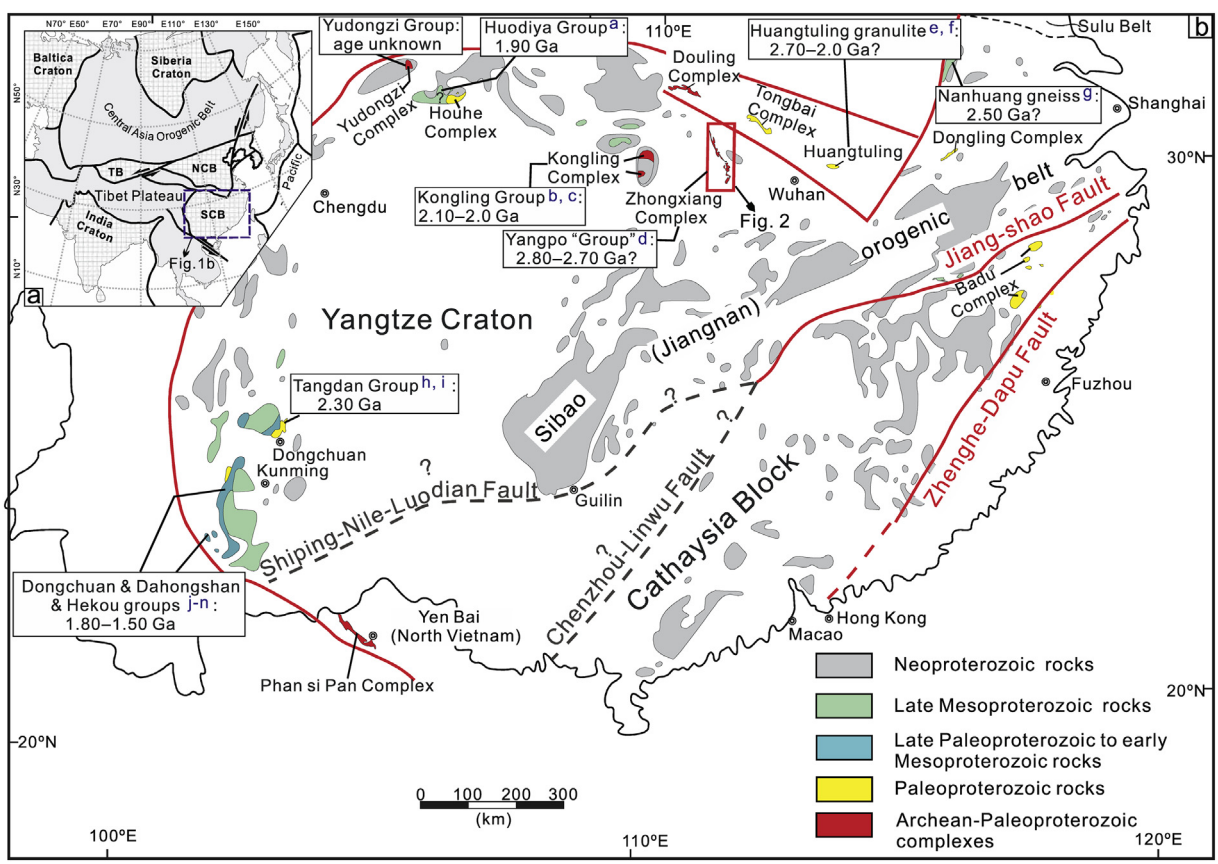

Fig. 1. (a)Simplified tectonic map of Eurasia showing major tectonic units and the location of the SCB– South China Block, TB– Tarim Block, and NCB– North China Block (modified after Ge et al., 2014). (b)A simplified geological map highlighting the Precambrian geological units of south China (modified after Zhao and Cawood, 2012). Archean-Paleoproterozoic volcanic-sedimentary outcrops in the Yangtze Craton are marked with corresponding age estimates. Geochronological data are cited from a: J.Y. Li's unpublished data; b: Yin et al., 2013; c: Li et al., 2016; d: Wang et al., 2013a; e-f: Sun et al., 2008; Wu et al., 2008; g: Tu et al., 2001 (drilling core); h-i: Zhu et al., 2011; Zhou et al., 2012; j-n: Greentree and Li, 2008; Zhao et al., 2010; Zhao and Zhou, 2011; Chen et al., 2013b; Wang and Zhou, 2014.

Table 1
Summary of zircon U—Pb and Hf model ages of Archean magmatic rocks in the Yangtze Craton, South China.

Area	Lithology	Crystallization age (Ma)	Method	T^{C}_{DM} (Ga)	Data source
Kongling Complex	Gneiss	2936 ± 98	U-Pb (discordia upper intercept)		Ames et al., 1996
	Trondhjemitic gneiss	2947 ± 5	SHRIMP U-Pb	3.11	Qiu et al., 2000
	Trondhjemitic gneiss	2903 ± 10	SHRIMP U-Pb	3.07	
	Migmatite	2916 ± 31	SHRIMP U-Pb	3.30–3.70	Zhang et al., 2006
	Migmatite	2947 ± 28	SHRIMP U—Pb (discordia upper intercept)	3.30–3.70	
	Trondhjemitic gneiss	2930 ± 44	SHRIMP U-Pb	3.30–3.60	
	Migmatite	2936 ± 28	SHRIMP U-Pb		
	Gneiss	3218 ± 13	LA-ICPMS U-Pb	3.40–3.80	Jiao et al., 2009
	Garnet amphibolite	2857 ± 8	LA-ICPMS U-Pb	2.90–3.80	Wu et al., 2009
	Granodioritic gneiss	3262 ± 27	LA-ICPMS U-Pb		Gao et al., 2011
	Granodioritic gneiss	3234 ± 15	LA-ICPMS U-Pb		
	Granodioritic gneiss	2951 ± 20	LA-ICPMS U-Pb	3.40–3.80	
	Granitic gneiss	2645 ± 15	LA-ICPMS U-Pb	2.80–3.0	Chen et al., 2013a
	Granitic gneiss	2622 ± 14	LA-ICPMS U-Pb	2.80–3.10	
	Granitic gneiss	2640 ± 18	LA-ICPMS U-Pb	2.70–3.10	
	Granitic gneiss	2671 ± 17	LA-ICPMS U-Pb	2.70–3.50	
	Granitic gneiss	2691 ± 32	LA-ICPMS U-Pb	3.0–3.20	
	Granitic gneiss	2707 ± 24	LA-ICPMS U-Pb	3.0–3.30	
	Granitic gneiss	3229 ± 42	LA-ICPMS U-Pb	3.50–3.70	
	Granitic gneiss	2904 ± 31	LA-ICPMS U-Pb	3.30–3.50	
	Trondhjemitic gneiss	2909 ± 30	LA-ICPMS U-Pb	3.20–3.40	
	Trondhjemitic gneiss	2937 ± 16	LA-ICPMS U-Pb	3.10–3.30	
	Trondhjemitic gneiss	2907 ± 15	LA-ICPMS U-Pb	3.30–3.50	
	Granitic gneiss	3442 ± 8	LA-ICPMS U-Pb	3.60–4.10	Guo et al., 2014
	Granitic gneiss	3435 ± 7	LA-ICPMS U-Pb	3.60–4.10	
	Amphibolite	2945 ± 13	LA-ICPMS U—Pb (discordia upper intercept)		Li et al., 2014
	Trondhjemite	3313 ± 30	LA-ICPMS U—Pb (discordia upper intercept)	3.60–3.80	Guo et al., 2015
	Trondhjemite	3292 ± 33	LA-ICPMS U—Pb (discordia upper intercept)	3.60–3.80	
	Biotite-granite	2810 ± 48	LA-ICPMS U—Pb (discordia upper intercept)	3.30–3.50	
	Biotite-granite	2803 ± 27	LA-ICPMS U—Pb (discordia upper intercept)	3.30–3.40	
	Biotite-granite	2785 ± 43	LA-ICPMS U—Pb (discordia upper intercept)	3.20–3.60	
	Biotite-granite	2781 ± 26	LA-ICPMS U—Pb (discordia upper intercept)	3.30–3.50	
	Two-mica granite	2695 ± 23	LA-ICPMS U—Pb (discordia upper intercept)	3.0–3.10	
	Biotite-granite	2662 ± 20	LA-ICPMS U—Pb (discordia upper intercept)	3.20–3.50	
	Two-mica granite	2638 ± 26	LA-ICPMS U—Pb (discordia upper intercept)	3.10	
	Two-mica granite	2636 ± 51	LA-ICPMS U—Pb (discordia upper intercept)	3.10–3.40	
	Two-mica granite	2418 ± 52	LA-ICPMS U—Pb (discordia upper intercept)	3.40–3.50	
Zhongxiang Complex	Granite	2652 ± 21	LA-ICPMS U-Pb		Wang et al., 2013a
	Granite	2655 ± 9	SHRIMP U-Pb		Wang et al., 2013b
	Granite	2656 ± 6	LA-ICPMS U-Pb	3.10–3.30	Zhou et al., 2015
	Trondhjemitic gneiss	2771 ± 19	LA-ICPMS U-Pb	3.20–3.50	Wang et al., 2018
	Monzogranite	2897 ± 15	LA-ICPMS U-Pb	3.10–3.70	
	Monzogranite	2874 ± 24	LA-ICPMS U-Pb	2.80–3.60	
	Granite	2669 ± 18	LA-ICPMS U-Pb	2.90–3.30	
	Granite	2619 ± 30	LA-ICPMS U-Pb	3.0–3.30	
	Granite	2655 ± 13	LA-ICPMS U-Pb	3.10–3.30	
Yudongzi Complex	Granite	2693 ± 9	U-Pb (discordia upper intercept)		Zhang et al., 2001
	Mylonitic granite	2661 ± 17	LA-ICPMS U-Pb		Zhang et al., 2010
	Gneissic granite	2703 ± 26	LA-ICPMS U-Pb		
	Quartzite	2645 ± 25	LA-ICPMS U-Pb		Wang et al., 2011
	Trondhjemitic gneiss	2815 ± 18	LA-ICPMS U—Pb (discordia upper intercept)	2.80–3.10	Hui et al., 2017
	Amphibole plagiogneiss	2692 ± 26	LA-ICPMS U—Pb (discordia upper intercept)	2.90–3.10	
	Biotite plagiogneiss	2449 ± 4	LA-ICPMS U—Pb (discordia upper intercept)	2.80–3.10	
Douling Complex	Amphibole plagiogneiss	2469 ± 22	LA-ICPMS U—Pb (discordia upper intercept)		Hu et al., 2013
	Amphibole plagiogneiss	2479 ± 12	LA-ICPMS U—Pb (discordia upper intercept)	3.0–3.40	
	Plagiogneiss	2497 ± 27	LA-ICPMS U—Pb (discordia upper intercept)	2.70–3.20	
	Granitic gneiss	2501 ± 17	LA-ICPMS U—Pb (discordia upper intercept)	3.10–3.30	
	Biotite plagiogneiss	2509 ± 14	LA-ICPMS U—Pb (discordia upper intercept)	3.00–3.30	
	TTG gneiss	2509 ± 21	LA-ICPMS U-Pb	3.10–3.30	Wu et al., 2014
	TTG gneiss	2496 ± 15	LA-ICPMS U-Pb	3.10–3.30	
	Orthogneiss	2446 ± 12	LA-ICPMS U-Pb		Nie et al., 2016
	Orthogneiss	2433 ± 9	LA-ICPMS U-Pb		
	Orthogneiss	2478 ± 10	LA-ICPMS U-Pb		
North Vietnam	Orthogneiss	2834 ± 12	LA-ICPMS U—Pb (discordia upper intercept)		Lan et al., 2001
	Orthogneiss	2834 ± 27	LA-ICPMS U—Pb (discordia upper intercept)		
	Orthogneiss	2913 ± 10	SHRIMP U-Pb		Nam et al., 2003
	Orthogneiss	2835 ± 6	SHRIMP U-Pb		
	Orthogneiss	2843 ± 8	SHRIMP U-Pb		

Mesoproterozoic rocks locally distributed in the Archean-Paleoproterozoic Kongling and Zhongxiang complexes and the Archean Yudongzi and Douling complexes in the northern Yangtze Craton, the Dongchuan region in the southwestern Yangtze Craton, and the Archean-Paleoproterozoic orthogneiss complexes in North Vietnam on the southern Yangtze margin (Fig. 1b). The Kongling Complex, as the

oldest continental nuclei of the Yangtze Craton, was formed through two major episodes of sodic TTG magmatism at 3.45–3.43 Ga and 3.30–2.90 Ga, and two generations of relatively potassic granitoid magmatism at 2.80–2.70 Ga and 2.70–2.60 Ga (Table 1; Guo et al., 2015 and references therein). Outside the Kongling Complex, the oldest magmatic rocks were recently documented in the Zhongxiang Complex, which includes granitic rocks emplaced at 2.90–2.87 Ga, 2.77 Ga, and 2.67–2.62 Ga (Table 1; Wang et al., 2018). Other granitic rocks and orthogneisses with ages of 2.90–2.50 Ga are distributed within the Yudongzi and Douling complexes, and the Phan Si Pan Complex in North Vietnam(Fig. 1; Table 1; e.g.,Lan et al., 2001; Wu et al., 2014; Hui et al., 2017).

Associated with the Archean magmatic rocks are metasedimentary assemblages that occur as small lens and boudins (Fig. 1b). These are typically represented by the Yudongzi metasedimentary rocks that were poorly dated (Qin et al., 1992; Zhang et al., 2001), the Kongling high-pressuregranulite-facies metasedimentary rocks with protolith formation age recently dated to be 2.10–2.0 Ga (Li et al., 2016; Yin et al., 2013), the high-pressuregranulite-facies Huangtuling granulites with depositional age of the protoliths poorly constrained between 2.70 and 2.0 Ga by the ages of the youngest detrital zircons and the metamorphic overprint (Sun et al., 2008; Wu et al., 2008), and metasedimentary rocks within the Zhongxiang Complex which were initially defined as Proterozoic but have recently been demonstrated to be of Neoarchean age as they were intruded by Neoarchean granitic rocks (Wang et al., 2013a, 2013b; Zhou et al., 2015). In the southwestern Yangtze Craton, low-grade slates of the Paleoproterozoic Tangdan Group (2.30 Ga; Zhu et al., 2011; Zhou et al., 2012) sporadically crop out and are unconformably overlain by the Paleo- to Mesoproterozoic Dongchuan Group and its equivalents, the Dahongshan and Hekou groups (1.80–1.50 Ga; e.g.,Greentree and Li, 2008; Zhao et al., 2010; Chen et al., 2013b; Wang and Zhou, 2014; Wang et al., 2014), which comprise non-metamorphosed to low-gradevolcanic-sedimentary successions developed in rift-related settings.

2.2. Geology of the Zhongxiang Complex

The Zhongxiang Complex is exposed as a near NS-trending narrow belt along the west bank of the Hanshui River of the Zhongxiang County (Fig. 2a). This complex is generally subdivided into the northern and southern parts (Fig. 2a). In the southern Zhongxiang Complex, five granitic bodies were identified (HIGS, 2001). These granitic bodies have diverse lithologies and show varied crystallization ages, including 1.85 Ga K-feldspar granites, rapakivi granites, and monzogranites from the northern part of the Huashanguan pluton (Zhang et al., 2011; Zhou et al., 2017), 1.98–1.93 Ga K-feldspar granites from the southern part of the Lengshui pluton (Wang et al., 2015), 2.77 Ga trondhjemitic gneisses from the southern part of the Huashanguan pluton, and 2.90–2.87 Ga monzogranites from the Huachong intrusion (Wang et al., 2018). The northern part comprises a metasedimentary rock complex, termed the Yangpo "Group" (BGMRHP, 1990; HIGS, 1965), and some Neoarchean granitic bodies (2.67–2.62 Ga; Wang et al., 2013a, 2013b; Zhou et al., 2015; Wang et al., 2018) (Fig. 2b). The Yangpo "Group" consists mainly of quartz schist, metapelite, granulite, and plagioclase gneiss, which show highly variable metamorphic grades representing different structural levels of the crust or imprints of different tectonothermal events (BGMRHP, 1990; HIGS, 1965). Available U—Pb age data from detrital zircons, though limited, indicated a Neoarchean protolith age for the Yangpo quartz schists (2.80–2.70 Ga, Wang et al., 2013a).

Metapelites of the Yangpo "Group" are strongly deformed with primary sedimentary layering modified or completely replaced by lineation and foliation. Field observations show an intrusive contact between the stock-like granite intrusions and the metapelites, both of which are either unconformably overlain by, or in fault contact with, Sinian diamictites. The metapelites exhibit gneissic structures and amphibolite-facies mineralogical assemblages (garnet-sillimanite-biotite gneisses; Fig. 3), with a consistent mineral composition including quartz, biotite, plagioclase, and K-feldspar, with minor sillimanite, garnet, staurolite, and muscovite. Quartz grains are elongated and parallel

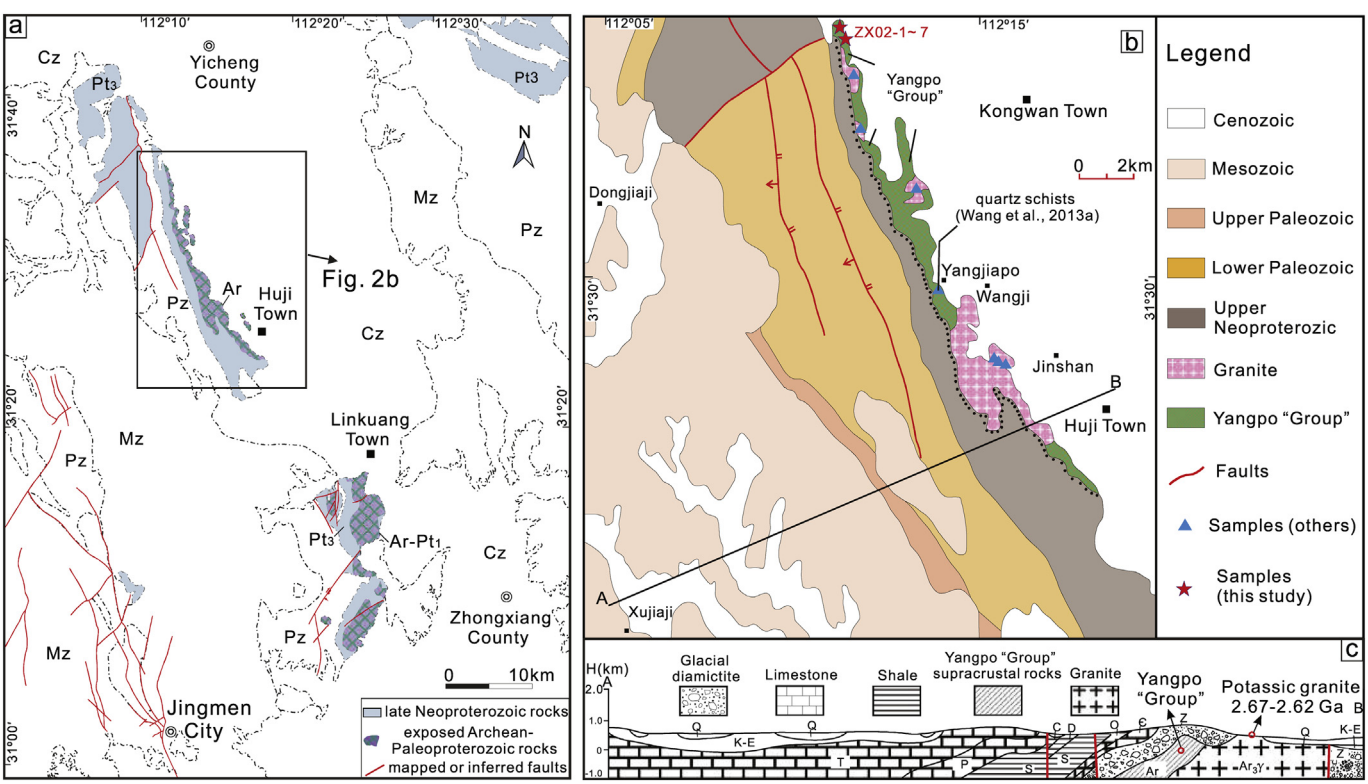

Fig. 2. (a)Simplified geological map of the Archean-Paleoproterozoic Zhongxiang Complex. (b)Schematic geological map of the northern Zhongxiang Complex showing sample locations. (c)Schematic cross section showing basic structures of the study area. Maps are modified after 1:200,000 geological maps of the Zhongxiang County and the Yicheng County. Geochronological samples of previous studies are cited from Wang et al. (2013a, 2013b), Zhou et al. (2015) and Wang et al. (2018).

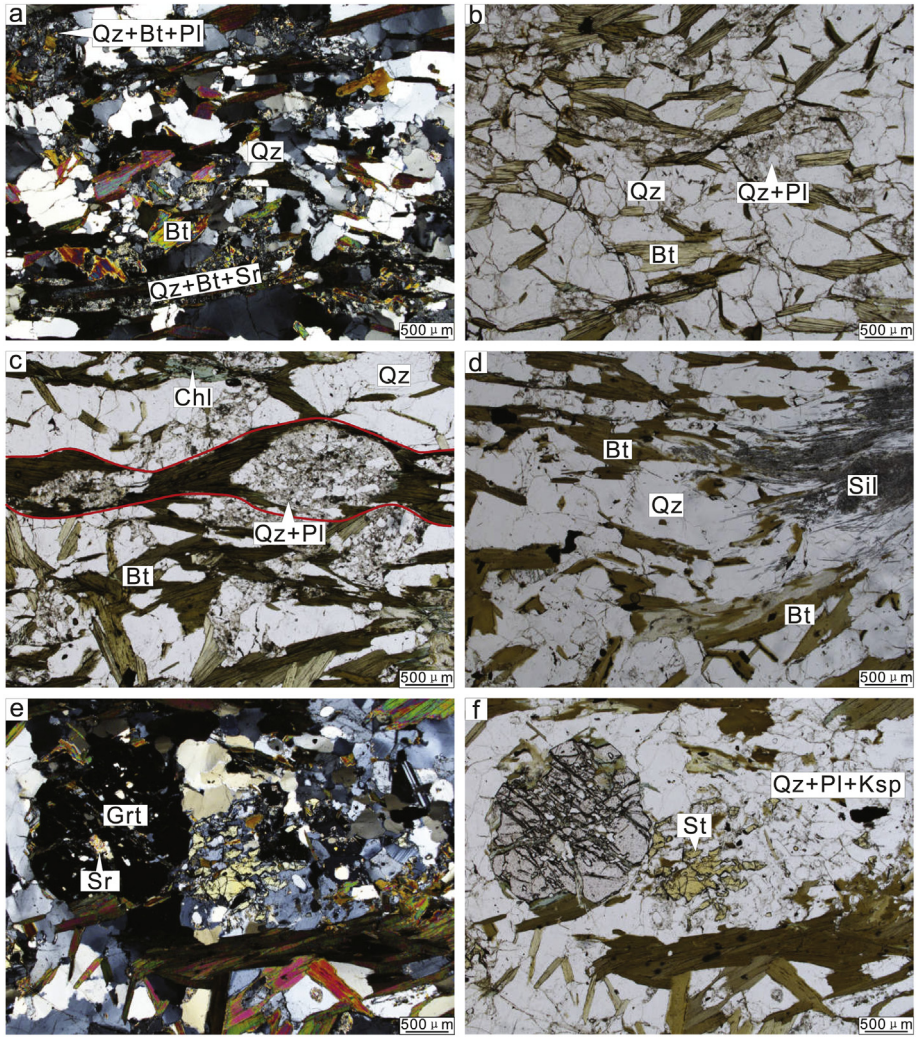

Fig. 3. Photomicrographs showing typical textures and mineral assemblages of metapelites from the Yangpo "Group". Mineral abbreviations are as follows: Qz = quartz, Bt = biotite, Pl =plagioclase, Ksp = K-feldspar, Sr = sericite, Chl = chlorite, Sil = sillimanite, Grt = garnet, St = staurolite. (a)and (e)in crossed Nicols, all others in open Nicols.

to the foliation (Fig. 3a, b). Plagioclase shows alteration to sericite (Fig. 3a). Fine-grained biotite grains occur between quartz grains and show a preferred orientation (Fig. 3b, c). Biotite grains have been partly altered to chlorite (Fig. 3c). Pressure shadow composed of biotite grains points to strong deformation (Fig. 3c). Muscovite has been commonly replaced by biotite and sillimanite. Fibrous sillimanite aggregates show a weak preferred orientation (Fig. 3d). Garnet found in the rocks usually contains inclusions of fine-grained quartz and plagioclase (Fig. 3e, f).

3. Samples and analytical methods

Seven metapelite samples (ZX02–1–7) were collected from the same outcrop near the Kongwan Town (GPS: N31°35′37.0″, E112°11′47.9″) (Fig. 2b). Two samples (ZX02–1–2) were selected for detrital zircon U—Pb dating and Lu—Hf isotopic analysis, and the other five samples (ZX02–3–7) were selected for whole-rock chemical analysis.

3.1. Zircon U—Pb dating

Zircon grains were separated by standard rock crushing, heavy liquid, and magnetic techniques. >150 zircon grains from each sample were hand-picked under a microscope, the cathodoluminescence (CL) images of which were then obtained using a GatanCL attached to a scanning electron microscope (SEM) (JSM-6510, Japan) at the Beijing CreaTech Testing International Co., Ltd., Beijing, China. Grains with visible fractures and inclusions were avoided. Zircons were mounted in epoxy resin and polished to expose their cores. Based on transmitted-light and reflected-light microphotographs and CL images, in situ zircon U—Pb isotope analysis was carried out by an AnlyitikJena PQMS Elite ICP-MS (inductively coupled plasma mass spectrometry) instrument attached to an ESI NWR 193 nm laser ablation system at Beijing Createch Testing Technology Co.Ltd. Detailed operating conditions for the laserablation system, the ICP-MS instrument, and data reduction are the same as described in Hou et al. (2009). Zircon GEMOCGJ-1($^{207}Pb/^{206}Pb$ age of 608.5 ± 1.5 Ma) was used as the external standard and NIST 610 was analyzed every 5–10 analyses to normalize U, Th and Pb concentrations of the unknowns (Jackson et al., 2004). All analyses were carried out using a beam with a diameter of 25 μm and a repetition rate of 5 Hz. The original data were processed by the ICPMSDataCal (ver. 10.1) software (Liu et al., 2008, 2010), and U—Pb ages were processed by the ISOPLOT program (Ludwig, 2003).

3.2. Zircon Lu—Hf isotopes

In situ zircon Lu—Hf isotope analysis was conducted using a Neptune Plus Multiple Receiving Plasma Mass Spectrometer equipped with a Compex pro.193 nm UV laser ablation system (LA-MC-ICP-MS) at the Continental Tectonics and Dynamics Laboratory of Institute of Geology, Chinese Academy of Geological Sciences, Beijing. Lu—Hf spots

partly or totally overlap with the U—Pb dating spots. The working parameters of ablation pit 44 μm in diameters, 8 Hz repetition rate and 25 s ablation time were employed. Detailed instrumental conditions and data acquisition procedures are as in Hou et al. (2007). Reference standard GJ-1 yielding $^{176}Hf/^{177}Hf$ ratios comparable with the recommended $^{176}Hf/^{177}Hf$ ratio of 0.282008 ± 0.000025 (Hou et al., 2007) were used to monitor performance conditions and analytical accuracy. A decay constant of 1.865×10^{-11} a^{-1} for ^{176}Lu (Scherer et al., 2001) and the present-day chondritic values of $^{176}Hf/^{177}Hf = 0.282772$ and $^{176}Lu/^{177}Hf = 0.0332$ (Blichert-Toft and Albarède, 1997) were adopted for the calculation of initial Hf isotope ratios and $\varepsilon_{Hf}(t)$. Single-stage model age (T_{DM1}) was calculated using the measured $^{176}Lu/^{177}Hf$ ratios, referenced to a depleted mantle source with a $^{176}Hf/^{177}Hf$ ratio of 0.28325, similar to that of average mid-ocean ridge basalt (MORB; Nowell et al., 1998), and a $^{176}Lu/^{177}Hf$ ratio of 0.0384 (Griffin et al., 2002). Two-stage "crustal" model age ($\boldsymbol{T_{DM}^{C}}$) was calculated by projecting the initial $^{176}Hf/^{177}Hf$ of zircons back to the depleted mantle growth curve, assuming an average $^{176}Lu/^{177}Hf$ ratio of 0.015 for the bulk continent crust (Griffin et al., 2002).

3.3. Whole-rock chemistry

The samples were crushed into powder of <200 mesh size in an agate shatterbox. Whole-rock major and trace elements were then analyzed at the National Research Center for Geoanalysis, Beijing, China. Major oxides were determined by X-ray fluorescence spectrometer (XRF) (Rigaku-3080) with a precision better than 2% for all elements. Trace elements Zr, Nb, V, Cr, Sr, Ba, Zn, Ni, Rb, and Y were analyzed using a Rigaku-2100 with analytical errors <3–5%, whereas other trace elements including REE were measured by a quadrupole inductively coupled plasma mass spectrometry (ICP-MS) using a TJA PQExCell system. Each powdered sample was precisely weighed around 25 mg and then dissolved in a high-pressure Teflon bomb using an HF + HNO_3 mixture and heated to 190 °C for ~48 h. Two international standards (GSR-1 and GSD-9) were used for calibration of the analyses. The analytical discrepancy is <5% and 5–10% for elements with abundance >10 ppm and <10 ppm, respectively. The analytical procedure was described in He et al. (2002).

4. Results

4.1. Zircon U—Pb geochronology

Detrital zircon U—Pb dating results of the two metapelite samples are presented in Table 2. Only concordant ages ($^{207}Pb/^{206}Pb$ age within 95–105% concordance, hereafter) are taken as reliable and accepted for binned frequency histograms. The representative CL images of the analyzed zircons together with corresponding spot numbers, ages and $\varepsilon_{Hf}(t)$values (where available) are shown in Fig. 4.

Zircons separated from both samples have similar morphological and internal structure characteristics. A majority of the picked zircon grains are too small (long axes normally <50 μm) to be dated using the laser ablation method. The analyzable zircons are mostly colorless, transparent, and euhedral to subhedral, with lengths ranging between 50 and 150 μm. They generally have elongated prismatic or stubby shapes and abraded edges with aspect ratios ranging between 1.0 and 4.0, although some of them are sub-rounded(Fig. 4). The analyzed zircon grains show variable internal structures, with a majority of the grains containing zircon cores which have simple oscillatory zoning and some blurry, chaotic domains or planar zoning. Moreover, the analyzed zircon grains generally have relatively thin (5 to 60 μm) and unzoned outer rims (Fig. 4).

In total, from sample ZX02–1, 98 U-Pb analyses were obtained from 95 zircon cores, whereas no analysis was obtained from the rims that are generally too narrow to be dated. All the dated cores have Th/U ratios >0.40 (0.40–1.44), except for 11 spots with Th/U ratios of 0.02–0.33 (Table 2). Forty analyses yielded discordant ages plotting below the concordia curve, reflecting at least a Phanerozoic radiogenic Pb-loss event (Fig. 5a). A regional Pb-loss event (weighted mean = 422 ± 74 Ma, MSWD = 2.7; Fig. 5a inset), calculated using the lower intercept ages of four relatively well defined discordias and one concordant analysis with a similar age that resulted from a Pb-loss or metamorphic event, from the Archean granitic rocks in the Zhongxiang Complex (Wang et al., 2018), is considered here as one of the radiogenic Pb-loss event (Pb-loss 2)that affected both samples. Early-middle Paleozoic tectonism is yet not documented in the Zhongxiang Complex area, but coeval large-scale magmatism is recorded both in the Qinling orogenic belt to the north (Dong and Santosh, 2016) and in the Wuyi-Yunkai orogen to the southeast (Li et al., 2010, 2017). If grouped by apparent $^{207}Pb/^{206}Pb$ age, most of these discordant data are plotted along two poorly defined discordias with upper intercept ages of 2775 ± 15 Ma (MSWD = 0.23, N = 49) and 2883 ± 16 Ma (MSWD = 0.18, N= 41) (Fig. 5a). The remaining 58 analyses yielded concordant ages ranging between 3350 and 2695 Ma. Except for five older ages between 3350 and 2950 Ma, the other fifty-three concordant ages (2927–2695 Ma) display two prominent peaks at ca. 2875 Ma and ca.2780 Ma within major age groups of 2920–2850 Ma and 2820–2730 Ma, respectively (Fig. 5c).

For sample ZX02–2, 147 U-Pb analyses were conducted on both cores and rims from 135 zircons. The rims have extremely low Th (1−20) and variable U (94–681), with Th/U ratios being mostly <0.10 (0.01–0.03, except for spot 135 with Th/U = 0.20) (Table 2), typical of metamorphic origins. Twenty-one out of the twenty-nine analyses on zircon rims are plotted along a discordant line with an upper intercept age of 1984 ± 46 Ma (MSWD = 0.13) (Fig. 6a). Seven concordant analyses from the rims gave a weighted mean $^{207}Pb/^{206}Pb$ age of 1952 ± 43 Ma (MSWD = 0.21) (Fig. 6b) that is, within uncertainty, consistent with the upper intercept age and is interpreted to be the growing age of these zircon rims. By contrast, most zircon cores, irrespective of U—Pb ages, yielded Th/U ratios ≥0.40 (0.40–1.40), although some cores gave lower Th/U ratios between 0.28 and 0.05 (n = 6) (Table 2). Analyzed zircon cores in sample ZX02–2 yielded several discordant results that are plotted in the triangular zones defined by multiple and/or incomplete radiogenic Pb-loss events, of which the Pb-loss event 1 is inferred from the presence of the 1.95 Ga metamorphic overprinting (Fig. 5b). Thirty-six out of the forty-two discordant spots are roughly plotted along two discordias (grouped by apparent $^{207}Pb/^{206}Pb$ age) with upper intercept ages of 2778 ± 16 Ma (MSWD = 0.15, N = 39) and 2880 ± 15 Ma (MSWD = 0.52, N = 36) (Fig. 5b). Seventy-six analyses on the cores yielded concordant ages that are plotted as histograms and relative probability curves in Fig. 5d. These ages (3350–2680 Ma) form two major groups of 2920–2850 Ma and 2820–2730 Ma which conspicuously peaked at ca. 2872 Ma and ca. 2775 Ma, respectively, with two minor peaks at ca. 3068 Ma and ca. 3350 Ma also recognizable (Fig. 5d).

4.2. Zircon Lu—Hf isotopes

The results of Lu—Hf isotopic analyses on 71 concordant zircon cores, 12 discordant zircon cores (calculated using upper intercept ages), and 1 zircon rim are presented in Table 3. The thirteen analyzed mid-Mesoarchean to Paleoarchean (3370–2920 Ma) zircons have predominantly positive $\varepsilon_{Hf}(t)$values (+0.77 to +4.53) with four zircons showing slightly negative values between −5.30 and −0.61. Except for one analysis from ZX02–2 with an abnormally high $\varepsilon_{Hf}(t)$value of +19.96 for unknown reasons, this mid-Mesoarchean to Paleoarchean zircon group possesses the highest $\boldsymbol{T_{DM}^{C}}$ ages (3.12–3.80 Ga) among all the studied zircons (Table 3). For the middle to late Mesoarchean (2920–2850 Ma) zircons, all 25 analyses, including 2 on discordant zircons, show a continuous variation of $\varepsilon_{Hf}(t)$values from positive to negative (−5.16 to +2.59), corresponding to $\boldsymbol{T_{DM}^{C}}$ ages of 3.65–3.15 Ga. In contrast, the majority of the early Neoarchean (2820–2730 Ma) zircons

Table 2
LA-ICP-MS U—Pb dating results of detrital zircons in the Yangpo metapelites from the Zhongxiang Complex.

Spot	Isotope ratios and errors (±1σ)						Ages (Ma) and errors (±1σ)						Concordance (%)	Th (ppm)	U (ppm)	Th/U
	$^{207}Pb/^{206}Pb$		$^{207}Pb/^{235}U$		$^{206}Pb/^{238}U$		$^{207}Pb/^{206}Pb$		$^{207}Pb/^{235}U$		$^{206}Pb/^{238}U$					
Metapelite (ZX02–1)																
01	0.20557	0.00483	11.82171	0.33243	0.41298	0.00670	2872	38	2590	26	2229	31	84	86.92	219.47	0.396
02	0.20843	0.00760	10.20213	0.31013	0.35258	0.00589	2894	59	2453	28	1947	28	76	79.92	388.15	0.206
03	0.19477	0.00615	10.61009	0.26233	0.39211	0.00498	2783	52	2490	23	2133	23	84	196.84	368.78	0.534
04	0.21028	0.00422	13.46421	0.28449	0.46235	0.01462	2909	32	2713	20	2450	64	89	140.48	215.73	0.651
05	0.19541	0.00438	10.16494	0.34483	0.37334	0.00883	2788	37	2450	31	2045	41	81	96.17	302.01	0.318
06	0.19374	0.00875	12.08874	0.49228	0.45261	0.01425	2776	74	2611	38	2407	63	91	52.04	160.37	0.325
07	0.18970	0.01027	10.28660	0.43095	0.39326	0.01058	2740	90	2461	39	2138	49	85	81.74	187.13	0.437
08	0.19360	0.00507	8.66509	0.34501	0.32129	0.00786	2773	44	2303	36	1796	38	75	377.07	497.39	0.758
09	0.19105	0.00706	11.42928	0.31293	0.43152	0.00850	2752	55	2559	26	2313	38	89	73.06	187.27	0.390
10	0.19489	0.00312	14.94486	0.32946	0.55154	0.00708	2784	27	2812	21	2832	29	99	169.62	301.55	0.562
11	0.19333	0.00480	14.35091	0.27512	0.53598	0.01514	2772	41	2773	18	2767	64	99	93.73	210.15	0.446
12	0.19156	0.00556	13.99071	0.45120	0.52583	0.01088	2767	48	2749	31	2724	46	99	121.99	212.31	0.575
13	0.18823	0.01145	7.28497	0.35410	0.28075	0.00881	2728	95	2147	43	1595	44	70	65.46	366.15	0.179
14	0.18880	0.00552	11.19392	0.30862	0.42761	0.00819	2732	48	2539	26	2295	37	89	50.31	137.97	0.365
15	0.18838	0.00952	7.05343	0.30523	0.27153	0.00721	2728	83	2118	39	1549	37	68	18.70	173.79	0.108
16	0.19314	0.00901	5.46783	0.15700	0.20672	0.00784	2769	77	1896	25	1211	42	55	53.81	596.02	0.090
17	0.20629	0.00591	16.58895	0.41517	0.57955	0.00802	2877	47	2911	24	2947	33	98	138.39	144.20	0.960
18	0.19376	0.00471	13.89419	0.33064	0.51697	0.00738	2776	35	2743	23	2686	31	97	74.39	180.75	0.412
19	0.20803	0.00562	14.85834	0.37303	0.51491	0.00713	2890	77	2806	24	2678	30	95	196.29	203.07	0.967
20	0.19705	0.00428	14.96622	0.31985	0.54814	0.00761	2802	35	2813	20	2817	32	99	84.77	113.73	0.745
21	0.19214	0.00408	13.86662	0.29972	0.52059	0.00682	2761	35	2741	20	2702	29	98	72.13	119.51	0.604
22	0.18466	0.00513	13.03755	0.36186	0.50949	0.00734	2695	45	2682	26	2654	31	98	90.53	195.00	0.464
23	0.18984	0.00742	10.77575	0.38420	0.41003	0.00677	2743	64	2504	33	2215	31	87	67.15	212.42	0.316
24	0.19147	0.00477	14.20476	0.36815	0.53520	0.00722	2755	41	2763	25	2763	30	99	111.13	149.26	0.745
25	0.18832	0.00536	10.53078	0.36502	0.40239	0.00860	2727	47	2483	32	2180	40	87	176.89	328.37	0.539
26	0.18528	0.00694	7.15361	0.24659	0.27790	0.00470	2702	61	2131	31	1581	24	70	70.87	441.67	0.160
27	0.19167	0.00719	10.14419	0.44287	0.37962	0.01001	2756	62	2448	40	2075	47	83	92.41	164.50	0.562
28	0.18985	0.00499	11.41690	0.36350	0.43067	0.01015	2743	43	2558	30	2309	46	89	96.09	167.44	0.574
29	0.20680	0.00631	10.64413	0.39399	0.36763	0.00956	2881	49	2493	34	2018	45	78	253.61	394.56	0.643
30	0.21028	0.00754	15.76785	0.78221	0.53473	0.02064	2909	57	2863	47	2761	87	96	46.98	87.90	0.535
31	0.20518	0.01025	16.44881	0.70322	0.57247	0.03054	2868	81	2903	41	2918	125	99	128.31	161.61	0.794
32	0.19685	0.00650	11.59496	0.55464	0.41749	0.01689	2867	54	2572	45	2249	77	86	203.04	300.79	0.675
33	0.20773	0.00680	15.37656	0.68303	0.52473	0.02647	2888	52	2839	42	2719	112	95	143.94	283.37	0.508
34	0.18095	0.00766	6.93687	0.26721	0.27301	0.01550	2661	70	2103	34	1556	79	70	511.46	645.45	0.792
35	0.23553	0.00564	12.44184	0.54671	0.36002	0.02156	3090	38	2638	41	1982	102	71	132.80	376.58	0.353
36	0.20419	0.00834	11.38835	0.52635	0.39671	0.01421	2861	66	2555	43	2154	66	82	113.29	234.61	0.483
37	0.19397	0.00585	7.76839	0.24826	0.28941	0.01387	2776	50	2205	29	1639	69	70	667.88	462.38	1.444
38	0.18705	0.00522	8.56515	0.30120	0.32692	0.00835	2716	46	2293	32	1823	41	77	290.58	416.48	0.698
39	0.19231	0.00431	13.21430	0.36530	0.49148	0.00977	2762	37	2695	26	2577	42	95	81.50	179.74	0.453
40	0.20569	0.00499	10.22323	0.28864	0.35646	0.00722	2872	40	2455	26	1965	34	77	68.84	165.53	0.416
41	0.19400	0.00694	13.75723	0.53579	0.50938	0.01057	2776	59	2733	37	2654	45	97	44.82	120.34	0.372
42	0.19007	0.00483	11.05145	0.33682	0.41944	0.00727	2743	41	2527	28	2258	33	88	244.95	257.57	0.951
43	0.19183	0.00518	10.48343	0.31836	0.39473	0.00744	2758	44	2478	28	2145	34	85	172.62	256.78	0.672
44	0.19858	0.00526	14.19437	0.39731	0.51654	0.00857	2815	42	2763	27	2684	36	97	33.22	158.73	0.209
45	0.20828	0.00510	16.20057	0.42329	0.56253	0.01065	2892	39	2889	25	2877	44	99	41.16	152.74	0.270
46	0.19488	0.00440	13.80103	0.35097	0.51140	0.00729	2784	37	2736	24	2663	31	97	99.26	128.59	0.772
47	0.20441	0.00552	14.11689	0.47995	0.49850	0.00970	2862	44	2758	32	2607	42	94	117.60	256.74	0.458
48	0.12424	0.00521	2.96566	0.13118	0.17239	0.00404	2018	74	1399	34	1025	22	69	11.29	479.65	0.024
49	0.28501	0.00784	23.81794	0.68673	0.60286	0.01150	3390	43	3261	28	3041	46	93	208.31	253.88	0.821
50	0.19243	0.00314	11.63350	0.16272	0.43887	0.00896	2765	27	2575	13	2346	40	90	118.37	168.23	0.704
51	0.21027	0.00401	16.13935	0.34047	0.55693	0.01722	2909	31	2885	20	2854	71	98	142.31	119.93	1.187
52	0.20677	0.00366	15.89515	0.41581	0.55707	0.00914	2881	29	2871	25	2854	38	99	46.49	90.03	0.516
53	0.20816	0.00295	16.23061	0.42947	0.56488	0.01002	2891	23	2890	25	2887	41	99	70.13	97.44	0.720
54	0.20589	0.00226	16.24014	0.42077	0.57140	0.01169	2874	18	2891	25	2914	48	99	67.74	89.33	0.758
55	0.20698	0.00479	12.20845	0.27194	0.42861	0.01290	2883	38	2621	21	2299	58	86	125.10	138.15	0.906
56	0.20484	0.00281	12.41300	0.42055	0.43939	0.01843	2865	22	2636	32	2348	83	88	69.42	90.90	0.764
57	0.19535	0.00539	14.53730	0.39126	0.53971	0.01094	2788	45	2785	26	2782	46	99	55.10	85.16	0.647
58	0.21285	0.00283	17.09552	0.29602	0.58250	0.01315	2927	22	2940	17	2959	54	99	37.80	62.04	0.609
59	0.19198	0.00581	8.59630	0.41288	0.32374	0.00985	2759	50	2296	44	1808	48	76	144.46	219.18	0.659
60	0.20951	0.00312	16.35890	0.36493	0.56608	0.01928	2902	24	2898	21	2892	79	99	36.21	50.33	0.720
61	0.19416	0.00383	13.50782	0.36783	0.50476	0.01880	2777	32	2716	26	2634	81	96	172.83	139.57	1.238
62	0.20622	0.00373	15.99918	0.44439	0.56168	0.01041	2876	29	2877	27	2874	43	99	79.77	100.94	0.790
63	0.20456	0.00336	15.13101	0.27090	0.53623	0.01225	2863	32	2824	17	2768	51	98	84.19	129.69	0.649
64	0.19420	0.00321	13.76341	0.18463	0.51372	0.01084	2789	27	2734	13	2672	46	97	29.23	44.04	0.664
65	0.19324	0.00785	13.70217	0.31870	0.51508	0.01580	2770	67	2729	22	2678	67	98	63.61	89.03	0.714
66	0.20568	0.00779	12.50107	0.55035	0.44009	0.00919	2872	61	2643	41	2351	41	88	27.43	55.00	0.499
67	0.19218	0.00270	10.16151	0.23888	0.38307	0.01081	2761	22	2450	22	2091	50	84	105.79	199.30	0.531
68	0.20096	0.00393	13.76681	0.26883	0.49641	0.01251	2835	32	2734	18	2598	54	94	127.10	104.91	1.211
69	0.19418	0.00290	14.45115	0.35512	0.53892	0.00939	2789	24	2780	23	2779	39	99	40.05	66.53	0.602
70	0.19541	0.00410	13.58044	0.41473	0.50290	0.01057	2789	34	2721	29	2626	45	96	46.19	47.76	0.967
71	0.19110	0.00365	7.53397	0.29976	0.28614	0.01451	2752	31	2177	36	1622	73	70	192.62	249.36	0.772

Table 2 (*continued*)

Spot	Isotope ratios and errors (±1σ)						Ages (Ma) and errors (±1σ)					Concordance (%)	Th (ppm)	U (ppm)	Th/U
	$^{207}Pb/^{206}Pb$		$^{207}Pb/^{235}U$	$^{206}Pb/^{238}U$			$^{207}Pb/^{206}Pb$		$^{207}Pb/^{235}U$		$^{206}Pb/^{238}U$				
72	0.19644	0.00378	14.46488	0.21746	0.53408	0.01480	2798	31	2781	14	2759	62	99	63.04	64.18	0.982
73	0.20332	0.00382	15.43938	0.50742	0.54917	0.01032	2853	31	2843	31	2822	43	99	35.03	52.85	0.663
74	0.19293	0.00316	12.89804	0.20233	0.48425	0.01299	2769	27	2672	15	2546	56	95	100.06	106.59	0.939
75	0.20851	0.00508	16.80827	0.37544	0.58345	0.00692	2894	40	2924	21	2963	28	98	102.11	121.33	0.842
76	0.20149	0.00280	16.10829	0.39015	0.57810	0.00982	2839	22	2883	23	2941	40	98	48.66	105.12	0.463
77	0.20928	0.00328	15.61549	0.40267	0.54103	0.01812	2900	25	2854	25	2788	76	97	67.15	86.67	0.775
78	0.21968	0.00410	17.82663	0.49302	0.58660	0.01047	2989	31	2980	27	2976	43	99	42.34	66.04	0.641
79	0.20467	0.00374	16.29090	0.47292	0.57530	0.01194	2864	30	2894	28	2930	49	98	38.25	60.86	0.629
80	0.20558	0.00262	16.47458	0.40729	0.58041	0.01841	2872	21	2905	24	2950	75	98	123.36	104.87	1.176
81	0.20217	0.00867	15.42766	0.33946	0.55411	0.01789	2844	70	2842	21	2842	74	99	32.25	46.62	0.692
82	0.19432	0.00443	14.32334	0.48306	0.53302	0.01080	2779	37	2771	32	2754	45	99	120.88	108.58	1.113
83	0.20290	0.00276	13.16057	0.30761	0.46992	0.01405	2850	22	2691	22	2483	62	91	116.92	193.90	0.603
84	0.20886	0.00419	16.15114	0.36394	0.56097	0.01788	2898	32	2886	22	2871	74	99	33.48	41.29	0.811
85	0.20476	0.00288	16.04609	0.32332	0.56960	0.01560	2865	22	2880	19	2906	64	99	55.54	72.20	0.769
86	0.19641	0.00280	13.77453	0.19123	0.50829	0.01011	2798	23	2734	13	2649	43	96	64.53	72.25	0.893
87	0.20575	0.00335	16.25183	0.20197	0.57263	0.01088	2873	26	2892	12	2919	45	99	51.66	76.32	0.677
88	0.20906	0.00396	16.07038	0.32351	0.55782	0.01606	2898	25	2881	19	2858	66	99	72.37	94.14	0.769
89	0.21819	0.00477	17.84415	0.51722	0.59224	0.01054	2969	35	2981	28	2998	43	99	37.85	31.87	1.188
90	0.20672	0.00291	16.28238	0.22696	0.57082	0.00982	2880	23	2894	13	2911	40	99	46.11	76.49	0.603
91	0.22848	0.00378	18.94802	0.30151	0.60092	0.01167	3042	27	3039	15	3034	47	99	14.87	27.11	0.549
92	0.20759	0.00331	15.90454	0.38637	0.55466	0.00935	2887	26	2871	23	2845	39	99	38.29	55.94	0.684
93	0.19404	0.00290	14.33491	0.32942	0.53481	0.00939	2777	24	2772	22	2762	39	99	110.27	141.78	0.778
94	0.21569	0.00315	17.55229	0.47895	0.58902	0.01206	2950	23	2966	26	2985	49	99	45.78	46.26	0.990
95	0.27739	0.00631	23.63485	1.10256	0.61729	0.02198	3350	36	3253	45	3099	88	95	89.87	127.51	0.705
96	0.19953	0.00318	15.17566	0.23675	0.55097	0.01178	2833	27	2826	15	2829	49	99	28.20	53.87	0.524
97	0.20490	0.00321	14.62410	0.29732	0.51762	0.01478	2866	26	2791	19	2689	63	96	47.30	73.77	0.641
98	0.19205	0.00432	14.26380	0.31626	0.53876	0.01734	2761	37	2767	21	2778	73	99	34.40	60.30	0.570
Metapelite (ZX02–2)																
01	0.20596	0.01537	13.31566	0.89447	0.51716	0.01479	2874	122	2702	63	2687	63	99	69.40	157.46	0.441
02	0.20101	0.01345	10.23317	0.60706	0.41107	0.01134	2834	110	2456	55	2220	52	89	217.35	309.45	0.702
03	0.22989	0.01456	15.98613	0.87171	0.56321	0.01446	3052	102	2876	52	2880	60	99	117.74	246.47	0.478
04	0.18467	0.01113	7.32790	0.35401	0.32314	0.00630	2695	100	2152	43	1805	31	82	400.12	492.36	0.813
05	0.18532	0.01183	8.93314	0.42667	0.39654	0.00842	2701	106	2331	44	2153	39	92	195.83	261.59	0.749
06	0.19424	0.01362	8.83083	0.49893	0.37265	0.01015	2789	121	2321	52	2042	48	87	185.38	339.21	0.546
07	0.18368	0.01389	7.84807	0.44240	0.35119	0.00746	2686	120	2214	51	1940	36	86	239.23	377.17	0.634
08	0.11797	0.00743	5.49568	0.26720	0.33787	0.00873	1926	113	1900	42	1876	42	98	7.87	311.27	0.025
09	0.11888	0.00513	2.68107	0.08334	0.16227	0.00238	1939	77	1323	23	969	13	69	7.49	645.35	0.012
10	0.11838	0.00441	2.76262	0.09992	0.16705	0.00195	1932	67	1345	27	996	11	70	7.09	561.57	0.013
11	0.19474	0.00622	14.71644	0.42504	0.54055	0.00924	2782	53	2797	27	2786	39	99	99.01	175.14	0.565
12	0.19126	0.00659	14.63607	0.46192	0.54524	0.00890	2753	56	2792	30	2805	37	99	63.27	113.10	0.559
13	0.19084	0.00763	14.90781	0.49797	0.55539	0.00776	2750	65	2809	32	2848	32	98	94.81	156.03	0.608
14	0.19538	0.01043	15.14862	0.70424	0.54980	0.01122	2788	88	2825	44	2824	47	99	88.71	112.95	0.785
15	0.12083	0.00664	6.20148	0.33910	0.36009	0.00958	1968	66	2005	48	1983	45	98	3.19	128.17	0.025
16	0.18516	0.00383	11.14605	0.25453	0.43407	0.00577	2700	40	2535	21	2324	26	91	119.93	204.88	0.585
17	0.18427	0.00449	13.14962	0.36991	0.51485	0.01028	2692	40	2690	27	2677	44	99	22.44	66.03	0.340
18	0.18433	0.00371	10.05166	0.25515	0.39185	0.00654	2692	33	2440	24	2131	30	86	130.85	313.85	0.417
19	0.18970	0.00635	14.30846	0.41850	0.53574	0.00923	2740	55	2770	28	2766	39	99	159.20	261.29	0.609
20	0.18521	0.00639	8.75736	0.28846	0.33594	0.00696	2702	62	2313	30	1867	34	78	135.91	335.42	0.405
21	0.18953	0.00761	12.75606	0.42228	0.48063	0.01151	2738	65	2662	31	2530	50	94	106.58	229.35	0.465
22	0.19141	0.00604	14.78603	0.46620	0.55018	0.00960	2754	52	2802	30	2826	40	99	105.65	154.18	0.685
23	0.19337	0.00654	14.37981	0.48531	0.53184	0.00967	2772	56	2775	32	2749	41	99	41.17	97.81	0.421
24	0.20954	0.00647	16.82002	0.54115	0.57437	0.01068	2902	50	2925	31	2926	44	99	202.07	229.80	0.879
25	0.12054	0.00911	3.12410	0.21991	0.19917	0.02553	1965	131	1439	54	1171	137	79	11.63	580.99	0.020
26	0.20632	0.00533	16.23139	0.44731	0.56451	0.00828	2877	42	2891	26	2885	34	99	92.76	188.78	0.491
27	0.20635	0.00559	15.47759	0.42576	0.54182	0.00949	2877	44	2845	26	2791	40	98	22.56	37.21	0.606
28	0.18401	0.00379	8.38867	0.18367	0.32820	0.00406	2700	34	2274	20	1830	20	78	267.48	390.91	0.684
29	0.21898	0.00676	17.91173	0.93276	0.57519	0.01411	2973	49	2985	50	2929	58	98	45.95	97.32	0.472
30	0.12154	0.00327	2.25129	0.07273	0.13425	0.00349	1989	48	1197	23	812	20	61	9.37	681.13	0.014
31	0.20595	0.00494	15.01682	0.37048	0.52778	0.00848	2874	39	2816	23	2732	36	96	84.17	193.83	0.434
32	0.12124	0.00312	4.27221	0.10261	0.25464	0.00336	1976	46	1688	20	1462	17	85	10.49	419.94	0.025
33	0.19212	0.00368	14.29089	0.29641	0.53659	0.00643	2760	31	2769	20	2769	27	99	100.96	212.17	0.476
34	0.18563	0.00490	8.88349	0.43275	0.34445	0.01184	2706	43	2326	44	1908	57	80	251.00	429.05	0.585
35	0.18538	0.00431	12.46882	0.32539	0.48435	0.00650	2702	38	2640	25	2546	28	96	166.09	219.34	0.757
36	0.19065	0.00505	11.56503	0.28424	0.43715	0.00606	2748	44	2570	23	2338	27	90	163.72	338.46	0.484
37	0.18704	0.00729	10.42339	0.31086	0.40217	0.01575	2716	65	2473	28	2179	72	87	247.93	277.53	0.893
38	0.18800	0.00656	12.85321	0.43603	0.49179	0.00856	2725	57	2669	32	2578	37	96	138.83	258.68	0.537
39	0.19262	0.00384	14.21053	0.29289	0.53087	0.00611	2765	33	2764	20	2745	26	99	52.41	123.44	0.425
40	0.19263	0.00472	14.58481	0.39246	0.54538	0.01187	2765	41	2789	26	2806	50	99	62.59	122.77	0.510
41	0.19380	0.00353	14.98551	0.31613	0.55693	0.00817	2776	30	2814	20	2854	34	98	38.32	75.21	0.509
42	0.19319	0.00419	13.85753	0.28001	0.51646	0.00558	2769	30	2740	19	2684	24	97	94.79	137.60	0.689
43	0.18352	0.00747	8.61522	0.26662	0.33829	0.00452	2685	68	2298	28	1878	22	79	225.51	419.78	0.537
44	0.19146	0.00385	14.37180	0.31598	0.54094	0.00831	2755	33	2775	21	2787	35	99	82.62	145.26	0.569

(*continued on next page*)

Table 2 (*continued*)

Spot	Isotope ratios and errors (±1σ)						Ages (Ma) and errors (±1σ)						Concordance (%)	Th (ppm)	U (ppm)	Th/U
	$^{207}Pb/^{206}Pb$		$^{207}Pb/^{235}U$	$^{206}Pb/^{238}U$			$^{207}Pb/^{206}Pb$		$^{207}Pb/^{235}U$		$^{206}Pb/^{238}U$					
45	0.19296	0.00415	14.04126	0.34623	0.52422	0.00878	2768	35	2752	23	2717	37	98	144.58	196.53	0.736
46	0.20691	0.00665	15.93637	0.48190	0.55479	0.00751	2883	52	2873	29	2845	31	99	32.64	85.48	0.382
47	0.19471	0.00523	14.46189	0.45801	0.53414	0.01125	2782	43	2781	30	2759	47	99	104.40	152.66	0.684
48	0.20798	0.00652	12.54429	0.32172	0.43396	0.00784	2890	51	2646	24	2324	35	87	121.34	306.89	0.395
49	0.20760	0.00492	16.78774	0.46859	0.58017	0.01073	2887	39	2923	27	2949	44	99	55.49	114.84	0.483
50	0.20386	0.00757	15.20635	0.41747	0.53981	0.01853	2857	60	2828	26	2783	78	98	64.65	129.21	0.500
51	0.20766	0.00461	16.29364	0.40473	0.56202	0.01043	2887	37	2894	24	2875	43	99	161.56	219.91	0.735
52	0.20641	0.00561	16.55016	0.31480	0.57545	0.01371	2877	44	2909	18	2930	56	99	91.20	193.78	0.471
53	0.20723	0.01067	8.80792	0.26857	0.30992	0.01330	2884	84	2318	28	1740	65	71	282.99	412.76	0.686
54	0.20874	0.00527	16.56120	0.48067	0.56612	0.01211	2896	41	2910	28	2892	50	99	93.28	204.25	0.457
55	0.19210	0.00558	12.37903	0.48759	0.46002	0.01260	2760	42	2634	37	2440	56	92	46.74	126.17	0.370
56	0.23227	0.00789	14.68176	0.51920	0.45304	0.01042	3068	54	2795	34	2409	46	85	55.84	202.17	0.276
57	0.18952	0.00486	12.88906	0.34935	0.48911	0.00920	2738	42	2672	26	2567	40	96	57.97	150.47	0.385
58	0.19371	0.00555	14.20474	0.40635	0.52661	0.00805	2774	46	2763	27	2727	34	98	73.59	118.11	0.623
59	0.19649	0.00597	12.86466	0.40949	0.47071	0.00791	2797	50	2670	30	2487	35	92	289.05	341.16	0.847
60	0.19150	0.00558	12.18949	0.39000	0.45824	0.00811	2755	48	2619	30	2432	36	92	173.70	348.08	0.499
61	0.19267	0.00531	14.60368	0.41774	0.54754	0.00803	2765	45	2790	27	2815	33	99	86.09	150.92	0.570
62	0.19573	0.00611	14.16440	0.51034	0.52257	0.01012	2791	52	2761	34	2710	43	98	205.09	196.60	1.043
63	0.19222	0.00703	11.79812	0.41533	0.44377	0.00859	2761	60	2589	33	2367	38	91	51.14	118.70	0.431
64	0.23284	0.00669	19.72064	0.61453	0.61055	0.01092	3072	46	3078	30	3072	44	99	67.46	137.30	0.491
65	0.19065	0.00585	14.50322	0.44085	0.54705	0.00809	2748	50	2783	29	2813	34	98	60.70	141.64	0.429
66	0.18326	0.00617	13.27238	0.46407	0.51931	0.00904	2682	57	2699	33	2696	38	99	54.15	94.38	0.574
67	0.18499	0.00597	13.17794	0.38825	0.51012	0.00777	2698	53	2692	28	2657	33	98	120.23	185.91	0.647
68	0.18954	0.01038	12.39387	0.45732	0.48069	0.02162	2738	85	2635	35	2530	94	95	103.59	110.22	0.940
69	0.19158	0.00809	11.70518	0.39645	0.43389	0.00874	2767	69	2581	32	2323	39	89	80.45	449.59	0.179
70	0.20030	0.00526	14.91535	0.43560	0.54021	0.00990	2829	44	2810	28	2784	41	99	58.54	146.23	0.400
71	0.18542	0.00977	12.91862	0.71845	0.50899	0.01062	2702	87	2674	52	2652	45	99	118.50	160.85	0.737
72	0.19532	0.00906	14.08586	0.69905	0.52648	0.00820	2787	76	2756	47	2727	35	98	309.23	320.87	0.964
73	0.18982	0.00814	13.62821	0.64799	0.52314	0.00994	2740	71	2724	45	2712	42	99	120.57	216.38	0.557
74	0.21335	0.00821	10.41990	0.44348	0.35596	0.00804	2931	62	2473	39	1963	38	77	27.29	224.54	0.122
75	0.19070	0.00719	13.86224	0.54753	0.52964	0.01027	2750	62	2740	37	2740	43	99	63.10	132.68	0.476
76	0.20043	0.00603	15.23207	0.52326	0.55350	0.01110	2831	50	2830	33	2840	46	99	98.88	165.25	0.598
77	0.19216	0.00568	13.47365	0.37081	0.51838	0.02013	2761	43	2713	26	2692	85	99	161.27	281.10	0.574
78	0.28060	0.00969	22.93419	0.67969	0.59200	0.00920	3366	49	3224	29	2998	37	92	111.87	175.35	0.638
79	0.23464	0.00618	19.93660	0.56838	0.61374	0.01345	3084	42	3088	28	3085	54	99	113.67	104.75	1.085
80	0.19281	0.00438	12.02008	0.31194	0.44967	0.00745	2766	37	2606	24	2394	33	91	179.25	327.62	0.547
81	0.22217	0.00717	17.68183	0.59465	0.57502	0.01132	2998	52	2973	32	2928	46	98	109.95	120.62	0.912
82	0.21321	0.00560	16.30015	0.42618	0.55228	0.00752	2931	43	2895	25	2835	31	97	133.33	268.28	0.497
83	0.22297	0.00535	18.26793	0.43953	0.59277	0.00618	3002	38	3004	23	3001	25	99	129.38	224.18	0.577
84	0.22404	0.00633	12.97002	0.38603	0.41896	0.00673	3010	45	2677	28	2256	31	82	184.36	375.86	0.491
85	0.20890	0.00404	14.79156	0.38094	0.51047	0.00815	2898	31	2802	25	2659	35	94	133.76	212.08	0.631
86	0.20526	0.00683	15.93439	0.53394	0.56205	0.00809	2868	54	2873	32	2875	33	99	116.32	217.50	0.535
87	0.19607	0.00473	14.82324	0.45368	0.54803	0.01035	2794	40	2804	29	2817	43	99	75.30	66.97	1.124
88	0.20683	0.00337	15.86210	0.44848	0.55591	0.01200	2881	27	2869	27	2850	50	99	91.52	128.64	0.711
89	0.23170	0.00442	19.25690	0.77228	0.60186	0.01557	3064	31	3055	39	3037	63	99	62.83	64.88	0.968
90	0.20399	0.00181	15.05887	0.18867	0.53525	0.00857	2858	14	2819	12	2764	36	98	41.61	60.58	0.687
91	0.20510	0.00266	15.55492	0.26512	0.54971	0.00577	2878	21	2850	16	2824	24	99	119.80	165.29	0.725
92	0.19502	0.00346	11.98614	0.39156	0.44501	0.01048	2785	24	2603	31	2373	47	90	30.85	79.08	0.390
93	0.20919	0.00409	9.14122	0.29000	0.31748	0.01378	2899	26	2352	29	1777	67	72	118.21	257.27	0.459
94	0.19450	0.00239	9.76917	0.21137	0.36398	0.00599	2781	53	2413	20	2001	28	81	205.15	245.78	0.835
95	0.21089	0.00324	16.78507	0.32356	0.57686	0.00738	2913	26	2923	18	2936	30	99	87.81	62.85	1.397
96	0.21786	0.00461	15.87693	0.39512	0.52827	0.00823	2965	34	2869	24	2734	35	95	32.61	65.87	0.495
97	0.19280	0.00232	13.09938	0.26060	0.49236	0.00642	2766	21	2687	19	2581	28	95	85.40	133.95	0.638
98	0.27778	0.00335	24.67799	0.36952	0.64444	0.01213	3350	19	3296	15	3206	48	97	73.95	91.75	0.806
99	0.20548	0.00300	15.02637	0.25476	0.53104	0.01480	2870	23	2817	16	2746	62	97	69.83	89.69	0.779
100	0.20743	0.00515	13.44908	0.58717	0.46968	0.00949	2887	35	2712	41	2482	42	91	27.59	46.92	0.588
101	0.19894	0.00339	14.21072	0.41448	0.51771	0.00940	2818	32	2764	28	2689	40	97	89.06	148.03	0.602
102	0.12209	0.00257	4.63852	0.07353	0.27573	0.00678	1987	37	1756	13	1570	34	88	1.63	237.78	0.007
103	0.19423	0.00430	13.24656	0.46298	0.49428	0.01041	2789	36	2697	33	2589	45	95	63.84	120.59	0.529
104	0.20592	0.00845	11.31403	0.79823	0.39590	0.01479	2874	67	2549	66	2150	68	83	105.95	200.65	0.528
105	0.20514	0.00366	12.67369	0.14882	0.44823	0.00853	2868	29	2656	11	2387	38	89	146.00	132.20	1.104
106	0.19186	0.00407	11.25066	0.36179	0.42512	0.00760	2758	34	2544	30	2284	34	89	69.50	115.67	0.601
107	0.18768	0.00394	10.47780	0.19114	0.40515	0.00643	2722	40	2478	17	2193	30	87	166.02	208.71	0.795
108	0.20777	0.00278	14.89314	0.23596	0.52019	0.01225	2888	22	2808	15	2700	52	96	96.50	125.48	0.769
109	0.19301	0.00567	7.83873	0.31700	0.29630	0.01531	2768	48	2213	36	1673	76	72	77.00	279.48	0.276
110	0.19333	0.00370	14.74588	0.19728	0.55381	0.01126	2772	31	2799	13	2841	47	98	56.96	48.24	1.181
111	0.21718	0.00341	17.61181	0.55058	0.58715	0.01426	2961	25	2969	30	2978	58	99	34.84	48.40	0.720
112	0.19261	0.00389	14.22789	0.57347	0.53428	0.01418	2765	33	2765	38	2759	60	99	82.21	119.20	0.690
113	0.20534	0.00543	14.67368	0.62213	0.51741	0.01030	2869	48	2794	40	2688	44	96	40.82	78.97	0.517
114	0.21715	0.00417	16.38022	0.22713	0.54799	0.01235	2961	31	2899	13	2817	51	97	15.90	29.56	0.538
115	0.20728	0.00452	15.70728	0.52017	0.54895	0.01200	2884	35	2859	32	2821	50	98	64.31	84.61	0.760
116	0.12168	0.00263	3.73658	0.15200	0.22228	0.00779	1981	39	1579	33	1294	41	80	4.16	334.56	0.012
117	0.12025	0.00211	3.65286	0.05657	0.22012	0.00584	1961	31	1561	12	1283	31	80	1.18	258.34	0.005
118	0.12130	0.00408	4.65426	0.43943	0.28539	0.03639	1976	60	1759	79	1618	183	91	3.23	232.44	0.014

Table 2 (*continued*)

Spot	Isotope ratios and errors (±1σ)						Ages (Ma) and errors (±1σ)						Concordance (%)	Th (ppm)	U (ppm)	Th/U
	$^{207}Pb/^{206}Pb$		$^{207}Pb/^{235}U$		$^{206}Pb/^{238}U$		$^{207}Pb/^{206}Pb$		$^{207}Pb/^{235}U$		$^{206}Pb/^{238}U$					
119	0.20349	0.00404	15.95757	0.24904	0.56914	0.01241	2855	32	2874	15	2904	51	98	47.39	67.64	0.701
120	0.12143	0.00406	5.55301	0.12922	0.33222	0.01746	1977	60	1909	20	1849	84	96	1.00	96.82	0.010
121	0.12116	0.00328	3.60479	0.21450	0.21513	0.00832	1973	48	1551	47	1256	44	79	3.41	301.72	0.011
122	0.12131	0.00927	4.08634	0.63331	0.24310	0.02735	1976	137	1652	127	1403	142	83	3.63	271.06	0.013
123	0.12191	0.00255	3.96859	0.13903	0.23592	0.00512	1984	37	1628	28	1365	27	82	2.64	270.86	0.010
124	0.20329	0.00304	14.96673	0.35465	0.53375	0.00626	2853	24	2813	23	2757	26	97	53.10	99.52	0.534
125	0.19613	0.00426	12.23414	0.18860	0.45241	0.01087	2794	35	2623	14	2406	48	91	76.20	131.98	0.577
126	0.12072	0.00531	6.13707	0.55165	0.36762	0.02282	1969	78	1996	79	2018	108	98	1.70	200.66	0.008
127	0.12061	0.00337	2.81788	0.21167	0.16752	0.00858	1965	50	1360	56	998	47	69	10.56	350.76	0.030
128	0.19122	0.00607	12.48770	0.45211	0.47270	0.00805	2754	53	2642	34	2495	35	94	82.31	165.90	0.496
129	0.12733	0.00181	3.84996	0.04289	0.21897	0.00327	2061	25	1603	9	1276	17	77	4.84	289.54	0.017
130	0.15484	0.00477	4.85070	0.19643	0.22690	0.00617	2800	52	1794	34	1318	32	69	10.51	183.22	0.057
131	0.20474	0.00357	15.36573	0.42147	0.54318	0.01105	2865	28	2838	26	2797	46	98	24.49	44.65	0.548
132	0.12346	0.00235	3.84039	0.16560	0.22510	0.00835	2007	34	1601	35	1309	44	79	1.90	284.48	0.007
133	0.21099	0.00464	11.74337	0.51130	0.40137	0.01108	2913	37	2584	41	2175	51	82	104.49	170.83	0.612
134	0.20299	0.00388	14.97828	0.26234	0.53538	0.01536	2850	30	2814	17	2764	64	98	76.64	108.70	0.705
135	0.12499	0.00114	5.64977	0.16363	0.32725	0.00785	2029	21	1924	25	1825	38	94	20.14	101.87	0.198
136	0.12514	0.00217	4.89183	0.23810	0.28339	0.01812	2031	31	1801	41	1608	91	88	1.38	176.23	0.008
137	0.12704	0.00215	5.42727	0.11032	0.30957	0.01032	2058	29	1889	17	1739	51	91	1.71	94.37	0.018
138	0.23429	0.00509	11.39562	0.20475	0.35258	0.00848	3083	35	2556	17	1947	40	72	27.70	252.67	0.110
139	0.19334	0.00289	13.48591	0.34114	0.50699	0.01819	2772	25	2714	24	2644	78	97	128.64	168.95	0.761
140	0.12509	0.00154	6.66517	0.19766	0.38626	0.01430	2031	21	2068	26	2105	66	98	1.38	100.76	0.014
141	0.12555	0.00503	5.38822	0.37219	0.31092	0.01803	2037	71	1883	59	1745	89	92	1.04	108.12	0.010
142	0.12347	0.00175	4.45246	0.17647	0.26206	0.01171	2007	24	1722	33	1500	60	86	1.05	165.13	0.006
143	0.25725	0.00807	18.02369	0.58950	0.50790	0.00968	3231	50	2991	31	2648	41	87	76.06	179.39	0.424
144	0.12220	0.00304	3.73311	0.21333	0.22122	0.01019	1989	44	1578	46	1288	54	79	2.03	273.89	0.007
145	0.11709	0.00235	4.88341	0.25522	0.30284	0.02091	1922	36	1799	44	1705	103	94	2.60	250.02	0.010
146	0.12080	0.00439	5.57684	0.27047	0.33407	0.00851	1969	65	1913	42	1858	41	97	1.79	164.30	0.011
147	0.12361	0.00365	4.75544	0.20353	0.27860	0.00475	2009	47	1777	36	1584	24	88	1.00	122.89	0.008

gave negative $\varepsilon_{Hf}(t)$values between −5.56 and − 0.17, with only 5 out of 35 analyses showing positive $\varepsilon_{Hf}(t)$values (+0.34 to +2.24). Furthermore, zircon spot 62 for sample ZX02–2 yielded a highly enriched Hf-isotope composition ($\varepsilon_{Hf}(t) = -10.55$). The calculated $\boldsymbol{T_{DM}^{C}}$ ages of this early Neoarchean zircon group range between 3.58 and 3.11 Ga (except for spot 62 from sample ZX02–2 with $\boldsymbol{T_{DM}^{C}} = 3.92$ Ga). Among them, eight on the discordant zircon cores show similar $^{176}Hf/^{177}Hf$ ratios with similar-aged concordant zircons (Table 3), implying Pb-loss from the concordant zircons. For the youngest zircons with ages around 2700 Ma (2730–2680 Ma), 8 out of the 10 analyses gave negative $\varepsilon_{Hf}(t)$ values between −7.56 to −0.60, corresponding to $\boldsymbol{T_{DM}^{C}}$ ages of 3.65–3.28 Ga. The remaining two analyses gave positive $\varepsilon_{Hf}(t)$values of +1.90 and + 9.85, respectively.

4.3. Major and trace elements

Major and trace element compositions of the five metapelite samples of the Yangpo "Group" are presented in Table 4. A combination of the results from this study and previous work (on quartz schists, Wang et al., 2013a) are shown in Figs. 7–9.

The metapelite samples have low loss on ignition (LOI) values of <3%. They show a narrow range of almost all the major-element compositions (Table 4). They have SiO_2 (60.49–64.27 wt%), K_2O (1.02–2.37 wt %), Al_2O_3 (15.30–18.12 wt%), TiO_2 (0.82–0.93%), Fe_2O_3t (7.50–9.78 wt%) and MgO (3.28–5.06 wt%) contents that are comparable to those of the model chemical compositions of the average Archean upper continental crust (AUCC; $SiO_2 = 60.21$ wt%, $K_2O = 1.81$ wt%, $Al_2O_3 = 15.3$ wt%, $TiO_2 = 0.83$ wt%, $Fe_2O_3t = 8.89$ wt%, MgO = 4.69 wt%; Taylor and McLennan, 1995). Compared to the composition of the AUCC ($Na_2O = 3.30$ wt%), the metapelite samples show much lower abundances of Na_2O, ranging between 0.46 and 0.93 wt%. The samples are further characterized by slightly lower SiO_2/Al_2O_3 (3.34 to 4.09, average 3.85) but higher K_2O/Na_2O (1.32 to 3.61, average 2.19) ratios relative to the AUCC values ($SiO_2/Al_2O_3 = 3.94$, $K_2O/Na_2O = 0.55$). Our samples have exclusively negative discriminatory function (DF) values (Shaw, 1972) (Table 4), typical of metasedimentary rocks. On the Niggli index discrimination diagram (Winkler, 1976), geochemical compositions of the samples are all plotted in the pelitic rock field (Fig. 7a). Likewise, on the geochemical classification diagram of Herron (1988), they are all plotted in the shale area (Fig. 7b).

REE contents of the metapelite samples range from 148 to 277 ppm, with an average of 197 ppm higher than that of the quartz schist samples (mostly between 32 and 172 ppm, Fig. 8a; Wang et al., 2013a). The chondrite-normalizedREE plots show weakly fractioned light REE (LREE) relative to heavy REE (HREE) of the metapelites, with $(La/Yb)_N$ and $(Gd/Yb)_N$ ratios ranging from 2.95 to 7.05 and 1.11 to 1.46, respectively (Fig. 8a; Table 4). The HREEs are weakly fractionated with slightly inclined to flat patterns. The metapelite samples show negligibly to slightly negative Eu anomalies ($Eu/Eu^* = 0.76$–1.03, average 0.86; Table 4). All these geochemical characteristics are similar to those of the AUCC, which is characterized by a low REE content and $(La/Yb)_N$ ratio (<8), as well as a lack of Eu anomaly ($Eu/Eu^* \approx 1$) (Taylor and McLennan, 1985) (Fig. 8a). For the trace element, the samples have variable contents of Cr (33.10–592.0 ppm), Co (13.0–45.90 ppm) and Ni (23.20–2580 ppm) that are mostly higher than the AUCC values (Taylor and McLennan, 1985), and are characterized by equivalent Sc (20.10–29.10 ppm) and V (28.40–204.0 ppm) contents relative to the AUCC values (Table 4). The metapelites show highly variable large ion lithosphere elements (LILEs, e.g.,Rb: 45.0–98.4 ppm, Ba: 274.0–573.0 ppm, Sr: 75.70–173.0 ppm) that are generally higher than the AUCC(Taylor and McLennan, 1985) but lower than the UCC (upper continental crust; Rudnick and Gao, 2003) values. The samples have relatively uniform high field strength elements (HFSEs, e.g.,Nb: 6.48–21.40 ppm, Ta: 0.64–1.65 ppm, Zr: 130.0–372.0 ppm, Hf: 4.58–10.30 ppm), comparable with the AUCC values (Table 4). On the UCC-normalized spider diagram, however, the samples show

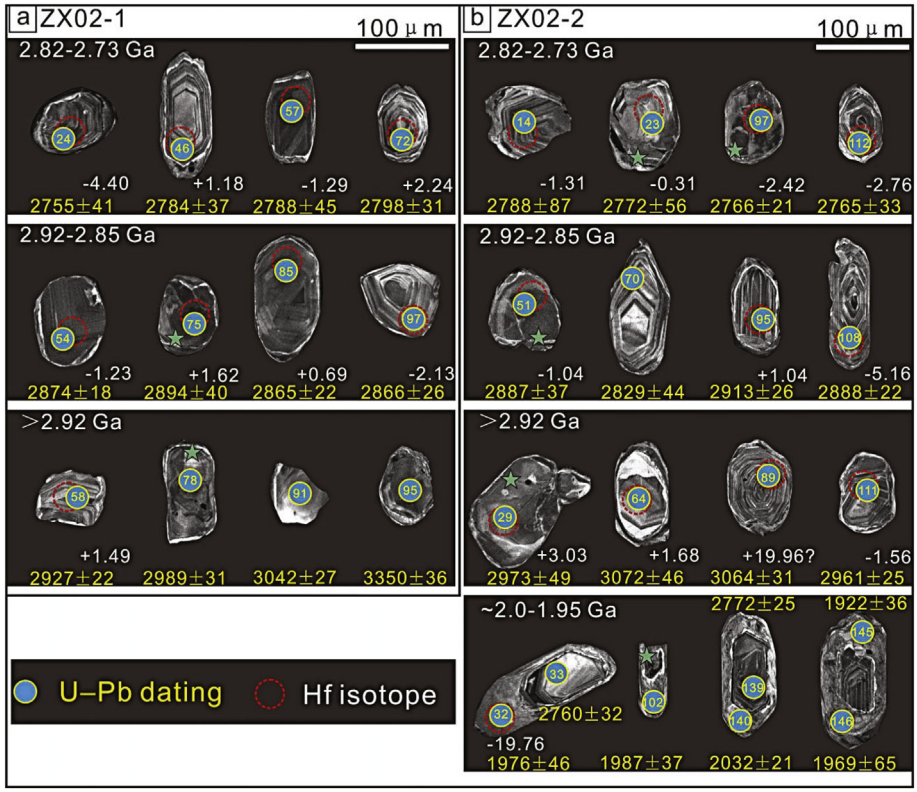

Fig. 4. CL images of representative zircon grains in the Yangpo metapelites, showing internal structures, analytical locations, calculated apparent $^{207}Pb/^{206}Pb$ ages (in yellow) and $\varepsilon_{Hf}(t)$ values (in white). Zircon grains with chaotic domains are marked with green stars. Numbers in yellow are spot numbers of U—Pb analyses.

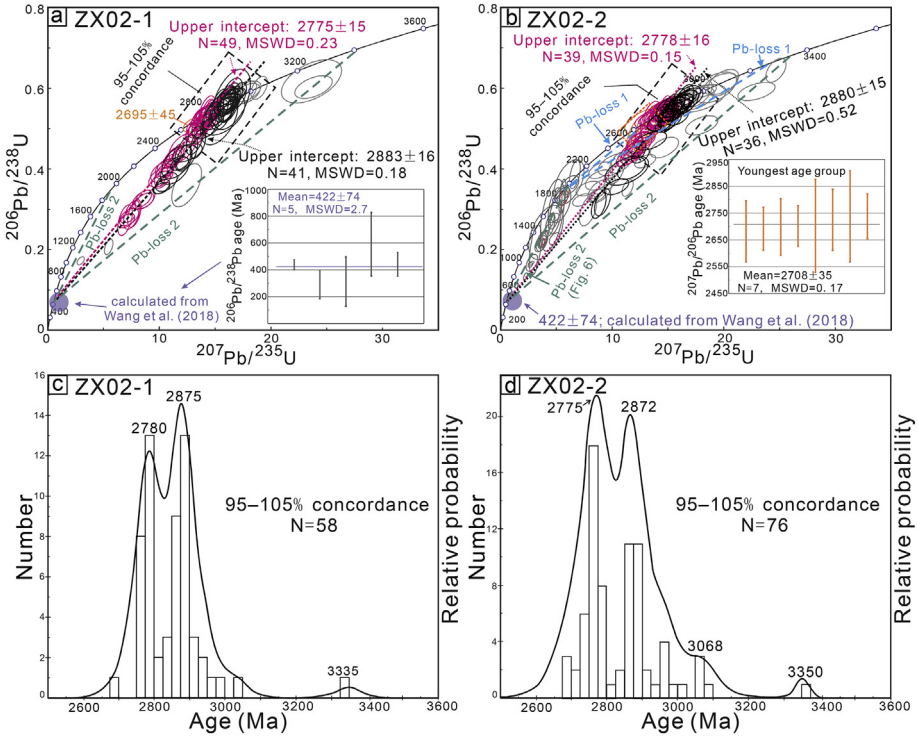

Fig. 5. (a–b) Concordia diagrams showing all zircon U—Pb ages of the Yangpo metapelites by LA-ICP-MS. The inset shows the $^{207}Pb/^{206}Pb$ ages of concordant analyses (95%–105% concordance) from the youngest magmatic cores, with the weighted mean age interpreted as the best estimates of the maximum depositional age of the protoliths of the metapelites. Two discordias are poorly defined for each sample by grouping the zircons with similar apparent $^{207}Pb/^{206}Pb$ ages. (c-d) Relative U—Pb age probability and histogram plots of the U—Pb age analyses within 95%–105% concordance.

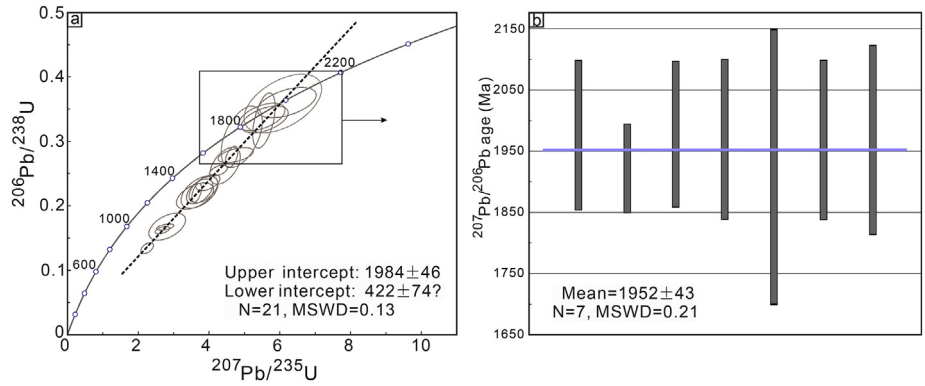

Fig. 6. (a)LA-ICP-MS zircon U—Pb age concordia plot of metamorphic zircons from metapelite sample ZX02–1, and (b)the $^{207}Pb/^{206}Pb$ ages of the concordant metamorphic zircons, with the weighted mean age interpreted as the best estimates of the metamorphic age of the Yangpo metapelites.

depletions in Sr and Tb (Fig. 8b), which are different from the AUCC(Taylor and McLennan, 1985).

5. Discussion

5.1. Depositional and metamorphic ages of the Yangpo metapelites

Detrital zircon grains have widely been used to constrain the depositional ages of sedimentary sequences, particularly those of Precambrian ages, in the absence of biostratigraphic age control (Fedo et al., 2003; Gehrels, 2012; Nelson, 2001). The metamorphic rocks of the Yangpo "Group" were previously considered to be Proterozoic in age (BGMRHP, 1990; HIGS, 1965), but recent U—Pb dating has suggested a Neoarchean protolith age for quartz schists of the Yangpo "Group" (2.80–2.70 Ga, Wang et al., 2013a).

Detrital zircon cores from the Yangpo metapelites (this study) have euhedral to subhedral and prismatic morphology as well as oscillatory zoning (Fig. 4) and are further characterized by high Th/U ratios (mostly >0.40; Table 2), all of which are suggestive of a magmatic origin. Thus, the youngest ages obtained from the detrital zircon cores can be used to place a maximum constraint on the depositional age of the protoliths of the Yangpo metapelites (e.g.,Fedo et al., 2003; Nelson, 2001). Whilst the youngest age group of 2.73–2.68 Ga only occurs in sample ZX02–2, sample ZX02–1 contains one concordant zircon that yielded a $^{207}Pb/^{206}Pb$ age of 2695 ± 45 Ma, which is identical, within error, with the weighted mean $^{207}Pb/^{206}Pb$ age (2708 ± 35 Ma, $N = 7$, MSWD = 0.17) for the youngest zircon group (Fig. 5b inset). The maximum protolith depositional age of the Yangpo metapelites is hereby estimated at 2.70 Ga. Combined with a direct constraint from the 2.67–2.62 Ga granitic bodies (Wang et al., 2018) intruding the Yangpo "Group", the protolith depositional age of the Yangpo metapelites can be tightly constrained between 2.70 and 2.67 Ga. Because the early study based on a geochronological study of the Yangpo quartz schists also presented several concordant detrital zircon $^{207}Pb/^{206}Pb$ ages around 2.70 Ga (Wang et al., 2013a), the age of 2.70–2.67 Ga perhaps represents the formation age of the protolith of the Yangpo "Group", which is therefore the oldest known sedimentary unit identified from the Yangtze Craton.

Dating of zircon rims from the Yangpo metapelites further documents an important metamorphic fingerprint at 1.95 Ga, which represents the first Paleoproterozoic metamorphic event reported from the northern Zhongxiang Complex. This metamorphic event appears to be younger than the 2.08 Ga metamorphic overprinting recorded in the Archean Youjiangchong trondhjemitic gneiss (Wang et al., 2018) but coincided with the 1.96–1.93 Ga arc-related granitic magmatism (Wang et al., 2015) in the southern Zhongxiang Complex. Combined with the younger (1.85 Ga) A-type granitic magmatism that is attributed to a late-collisional environment in the southern Zhongxiang Complex (Zhang et al., 2011; Zhou et al., 2017), we speculate that a Paleoproterozoic tectonic cycle involving 2.08 Ga subduction, 1.96–1.93 Ga (arc-continent?) collision, and 1.85 Ga late-collisional extension possibly took place in the Zhongxiang Complex area. In fact, Paleoproterozoic orogenic events have widely been documented in the Yangtze Craton (e.g.,Yin et al., 2013; Wang et al., 2015, 2016b; TableS1). A compilation of the Paleo- to Mesoproterozoic (2.20–1.40 Ga) metamorphic and magmatic age datasets for the Yangtze Craton, including the new data from this study, allows us to define two major episodes of metamorphism at 2.05–1.95 Ga and 1.86–1.82 Ga (Fig. 10a), and three major episodes of magmatism at 2.02–1.96 Ga, 1.86–1.82 Ga, and 1.75–1.68 Ga (Fig. 10b). The two metamorphic episodes, peaked at 2.0 Ga and 1.85 Ga, respectively, appear to be temporally associated with the older two episodes of magmatism which peaked at 1.98 Ga and 1.85 Ga, likely pointing to an extensive Paleoproterozoic orogenic reworking of the Yangtze Craton. While further interpretations of this orogenic event remain challenging given the fragmentary and incomplete nature of the ancient geologic record in the Yangtze Craton, this event can broadly be correlated with coeval late Paleoproterozoic (2.10–1.70 Ga) global orogeneses that led to the assembly of the supercontinent Nuna (also known as Columbia; Zhao et al., 2002; Evans et al., 2016).

5.2. Sedimentary environment

5.2.1. Post-depositional elemental mobility

The presence of secondary phases, such as sericite and chlorite (Fig. 3), indicates that the Yangpo metapelites have possibly experienced hydrothermal alteration and/or metamorphism since deposition. It is important to first evaluate the elemental mobility. Generally, alkali and alkaline earth elements and LILEs are expected to experience mobilization during alteration and metamorphism, whereas REEs, HFSEs, and some major oxides such as FeO, TiO_2, and Al_2O_3 are considered to be least affected by later alteration (e.g.,Bolhar et al., 2005; Taylor et al., 1986; Taylor and McLennan, 1985). The Yangpo metapelites show coherent REE patterns (Fig. 8a) and relatively uniform Nb/Ta (10.50–13.0) and Zr/Hf (27.70–36.30) ratios (Table 4), indicating that these immobile elements were not significantly changed. HFSEs Th and U are typically enriched in the crust due to igneous differentiation. While Th is a relatively immobile element, U is more easily affected by metamorphic dehydration and removed from the protoliths. The metapelites show a coherent behavior of Th and U, resulting in an average Th/U ratio of 3.30 ± 0.90 that is, slightly lower than the chondrite value (4.20) but significantly lower than typical dehydrated, high-grade metamorphic rocks (8.0–10.0) (Bolhar et al., 2005; Rudnick and Presper, 1990). These elementary features indicate that primary REE and HFSEs of our samples were not affected by metamorphism or hydrothermal alteration. Suspected immobile elements such as FeO,

Table 3
Hf isotopic compositions of detrital zircons in the Yangpo metapelites from the Zhongxiang Complex.

Spot[a]	$^{207}Pb/^{206}Pb$ Age (Ma)	Crystallization age (Ma)	$^{176}Hf/^{177}Hf$	2σ	$^{176}Lu/^{177}Hf$	2σ	$^{176}Yb/^{177}Hf$	2σ	$(^{176}Hf/^{177}Hf)^{b}$	$\varepsilon_{Hf}(0)$	$\varepsilon_{Hf}(t)^{c}$	2σ	T_{DM1} (Ma)	$T^{C}_{DM}{}^{d}$ (Ma)	2σ	$f_{Lu/Hf}{}^{e}$
Metapelite (ZX02–1)																
03	2783	2775	0.030554	0.000296	0.000952	0.000011	0.280996	0.000017	0.280945	−62.8	−2.25	0.62	3134	3379	24	−0.97
06	2776	2776	0.044872	0.000479	0.001392	0.000008	0.281074	0.000019	0.281000	−60.0	−0.26	0.69	3063	3253	27	−0.96
13	2728	2728	0.025669	0.000060	0.000732	0.000002	0.280936	0.000019	0.280898	−64.9	−5.03	0.68	3197	3519	26	−0.98
14	2732	2775	0.040942	0.000233	0.001562	0.000010	0.281052	0.000019	0.280969	−60.8	−1.39	0.68	3107	3324	26	−0.95
20	2802	2802	0.024558	0.000096	0.000839	0.000004	0.281013	0.000020	0.280968	−62.2	−0.83	0.69	3102	3309	26	−0.97
22	2695	2695	0.014676	0.000070	0.000455	0.000004	0.280960	0.000018	0.280937	−64.1	−4.40	0.64	3142	3454	24	−0.99
24	2755	2775	0.031838	0.000256	0.001000	0.000015	0.281071	0.000021	0.281018	−60.1	0.34	0.74	3036	3214	28	−0.97
29	2881	2883	0.020129	0.000118	0.000700	0.000004	0.281011	0.000021	0.280974	−62.3	−1.23	0.74	3093	3314	28	−0.98
31	2868	2868	0.027492	0.000366	0.000988	0.000015	0.280941	0.000016	0.280886	−64.8	−1.90	0.58	3212	3438	22	−0.97
36	2861	2883	0.061862	0.000523	0.001545	0.000017	0.281078	0.000020	0.280992	−59.9	1.93	0.69	3071	3195	27	−0.95
37	2776	2775	0.048251	0.000424	0.001624	0.000012	0.281039	0.000022	0.280949	−61.3	0.40	0.77	3130	3293	30	−0.95
38	2716	2775	0.096536	0.001659	0.002930	0.000031	0.281060	0.000025	0.280904	−60.6	−3.72	0.90	3213	3472	36	−0.91
42	2743	2775	0.038171	0.000199	0.001202	0.000005	0.281090	0.000021	0.281026	−59.5	0.61	0.76	3027	3196	29	−0.96
45	2892	2892	0.025663	0.000136	0.000812	0.000007	0.280962	0.000020	0.280919	−64.0	−3.91	0.71	3168	3460	27	−0.98
46	2784	2784	0.023595	0.000554	0.000695	0.000015	0.281004	0.000018	0.280965	−62.5	1.18	0.65	3103	3250	25	−0.98
54	2874	2874	0.038806	0.000394	0.001280	0.000011	0.280980	0.000029	0.280909	−63.4	−1.23	1.03	3183	3390	40	−0.96
57	2788	2788	0.016694	0.000327	0.000580	0.000010	0.280995	0.000027	0.280964	−62.9	−1.29	0.95	3106	3328	36	−0.98
58	2927	2927	0.017596	0.000083	0.000812	0.000004	0.280997	0.000031	0.280951	−62.8	1.49	1.09	3122	3257	41	−0.98
65	2770	2770	0.015936	0.000144	0.000695	0.000005	0.281063	0.000048	0.281026	−60.4	0.51	1.71	3023	3199	65	−0.98
68	2835	2835	0.019986	0.000392	0.000815	0.000014	0.281031	0.000034	0.280987	−61.6	0.63	1.21	3075	3241	46	−0.98
72	2798	2798	0.014766	0.000203	0.000526	0.000006	0.281085	0.000034	0.281057	−59.7	2.24	1.22	2981	3110	46	−0.98
75	2894	2894	0.042868	0.000270	0.001577	0.000009	0.281064	0.000047	0.280976	−60.4	1.62	1.66	3093	3223	64	−0.95
81	2844	2844	0.047597	0.000374	0.001652	0.000011	0.281067	0.000032	0.280977	−60.3	0.46	1.15	3095	3259	44	−0.95
82	2779	2779	0.022963	0.000244	0.000920	0.000008	0.280985	0.000020	0.280936	−63.2	−2.48	0.71	3146	3396	27	−0.97
85	2865	2865	0.048655	0.000282	0.001655	0.000010	0.281060	0.000030	0.280969	−60.5	0.69	1.08	3104	3261	42	−0.95
87	2873	2873	0.047981	0.000164	0.001724	0.000006	0.280940	0.000030	0.280845	−64.8	−3.54	1.08	3275	3536	42	−0.95
92	2887	2887	0.038040	0.000594	0.001358	0.000020	0.281026	0.000027	0.280951	−61.7	0.55	0.97	3126	3286	37	−0.96
97	2866	2866	0.031704	0.000483	0.001249	0.000020	0.280958	0.000043	0.280889	−64.2	−2.13	1.54	3210	3441	59	−0.96
Metapelite (ZX02–2)																
01	2874	2874	0.051820	0.000262	0.001277	0.000005	0.281054	0.000016	0.280984	−60.8	1.42	0.58	3081	3221	22	−0.96
03	3052	3052	0.022301	0.000342	0.000640	0.000007	0.280892	0.000014	0.280854	−66.5	0.96	0.49	3248	3387	18	−0.98
04	2695	2778	0.030316	0.000630	0.000952	0.000017	0.281046	0.000022	0.280990	−61.5	−0.60	0.69	3073	3276	26	−0.98
07	2686	2778	0.021372	0.000082	0.000680	0.000005	0.280999	0.000018	0.280979	−62.1	−0.97	0.86	3086	3300	32	−0.98
13	2750	2750	0.045874	0.000840	0.001436	0.000017	0.281081	0.000020	0.280996	−61.0	−1.04	0.78	3067	3282	30	−0.97
14	2788	2788	0.027876	0.000196	0.000861	0.000005	0.280894	0.000019	0.280963	−62.7	−1.31	0.65	3107	3329	24	−0.98
16	2700	2700	0.026400	0.000112	0.000831	0.000002	0.281065	0.000019	0.281007	−59.8	−1.81	0.71	3058	3293	27	−0.96
17	2692	2692	0.054251	0.000552	0.001539	0.000020	0.280998	0.000017	0.280850	−66.4	−7.56	0.69	3263	3652	26	−0.97
19	2740	2740	0.073309	0.000597	0.002003	0.000012	0.281078	0.000021	0.281021	−60.4	−0.36	0.69	3031	3231	26	−0.97
20	2702	2778	0.023746	0.000706	0.000731	0.000020	0.281057	0.000018	0.281002	−61.5	−0.17	0.66	3055	3249	25	−0.98
22	2754	2754	0.047102	0.001526	0.001312	0.000043	0.281014	0.000021	0.280917	−62.7	−3.73	0.61	3179	3457	24	−0.95
23	2772	2772	0.015103	0.000437	0.000478	0.000014	0.280979	0.000024	0.281002	−61.2	−0.31	0.65	3056	3253	25	−0.98
24	2902	2902	0.159467	0.002592	0.000558	0.000073	0.281138	0.000029	0.280994	−62.0	2.44	0.64	3063	3177	24	−0.99

29	2973	2973	0.071219	0.000326	0.001805	0.000006	0.281062	0.000022	0.280964	−59.9	3.03	0.73	3107	3194	29	−0.94
31	2874	2874	0.029849	0.000208	0.000884	0.000003	0.280989	0.000018	0.281017	−60.7	2.59	0.63	3034	3146	24	−0.98
32	1976	1984	0.001024	0.000028	0.000022	0.000001	0.281284	0.000022	0.280964	−62.2	−19.76	0.74	3139	3871	28	−0.96
34	2706	2778	0.026930	0.000273	0.000876	0.000010	0.281057	0.000024	0.280954	−63.4	−1.89	0.85	3119	3358	32	−0.99
35	2702	2702	0.027656	0.000446	0.000820	0.000010	0.281033	0.000019	0.281109	−57.8	1.90	1.03	2912	3058	39	−0.98
36	2748	2748	0.019697	0.000177	0.000715	0.000007	0.281017	0.000024	0.280967	−60.5	−2.10	0.80	3114	3348	31	−0.95
42	2769	2769	0.016711	0.000103	0.000599	0.000007	0.281034	0.000019	0.280942	−63.1	−2.52	0.63	3139	3391	24	−0.97
43	2685	2778	0.022925	0.000481	0.000738	0.000013	0.281041	0.000018	0.281283	−52.6	9.85	0.80	2678	2605	30	−1.00
44	2755	2755	0.014002	0.000144	0.000467	0.000003	0.281020	0.000018	0.281011	−60.7	−0.39	0.84	3046	3245	32	−0.97
46	2883	2883	0.036010	0.000653	0.001113	0.000014	0.281071	0.000018	0.281009	−60.2	2.54	0.65	3045	3156	25	−0.97
47	2782	2782	0.011061	0.000204	0.000327	0.000005	0.281001	0.000020	0.280983	−62.6	−0.74	0.71	3078	3288	26	−0.99
48	2890	2880	0.037817	0.000399	0.001109	0.000016	0.281064	0.000016	0.281002	−60.4	2.22	0.57	3055	3174	22	−0.97
51	2887	2887	0.068056	0.001106	0.002033	0.000021	0.281019	0.000022	0.280906	−62.0	−1.04	0.78	3193	3388	30	−0.94
52	2877	2877	0.025453	0.000190	0.000720	0.000002	0.280973	0.000017	0.280933	−63.6	−0.32	0.59	3146	3334	22	−0.98
56	3068	3068	0.070068	0.001088	0.002175	0.000045	0.280796	0.000021	0.280667	−69.9	−5.32	0.75	3515	3799	29	−0.93
57	2738	2738	0.037625	0.000403	0.001037	0.000015	0.281009	0.000020	0.280954	−62.4	−2.79	0.71	3124	3385	27	−0.97
58	2774	2774	0.055213	0.000482	0.001491	0.000013	0.281051	0.000023	0.280972	−60.9	−1.34	0.80	3103	3320	31	−0.96
59	2797	2797	0.038559	0.000466	0.001238	0.000017	0.280942	0.000020	0.280876	−64.7	−4.22	0.73	3231	3521	28	−0.96
60	2755	2755	0.030674	0.000083	0.000998	0.000008	0.281053	0.000018	0.281001	−60.8	−0.74	0.66	3060	3267	25	−0.97
61	2765	2765	0.067504	0.000189	0.001789	0.000011	0.281071	0.000023	0.280976	−60.2	−1.40	0.82	3101	3317	32	−0.95
62	2791	2791	0.026492	0.000379	0.000818	0.000012	0.280745	0.000018	0.280702	−71.7	−10.55	0.63	3459	3917	24	−0.98
64	3072	3072	0.012314	0.000146	0.000396	0.000004	0.280885	0.000020	0.280861	−66.7	1.68	0.70	3237	3356	26	−0.99
66	2682	2682	0.043675	0.000231	0.001214	0.000009	0.281039	0.000019	0.280915	−64.8	−5.48	0.65	3171	3513	24	−0.99
67	2698	2698	0.015812	0.000108	0.000493	0.000003	0.280940	0.000018	0.280976	−61.3	−2.94	0.68	3097	3364	26	−0.96
69	2767	2778	0.040835	0.000812	0.001210	0.000025	0.281013	0.000018	0.280949	−62.2	−2.07	0.63	3132	3369	24	−0.96
71	2702	2702	0.027033	0.000739	0.000914	0.000019	0.281039	0.000020	0.280992	−61.3	−2.28	0.72	3073	3325	27	−0.97
76	2831	2831	0.036823	0.000445	0.001009	0.000007	0.280999	0.000020	0.280945	−62.7	−0.97	0.73	3134	3340	28	−0.97
78	3366	3366	0.021163	0.000082	0.000661	0.000004	0.280626	0.000019	0.280584	−75.9	−1.33	0.68	3604	3774	25	−0.98
79	3084	3084	0.039330	0.001496	0.001368	0.000055	0.280870	0.000021	0.280789	−67.3	−0.61	0.74	3340	3512	28	−0.96
80	2766	2766	0.021720	0.000209	0.000698	0.000004	0.281030	0.000020	0.280858	−66.4	−5.56	0.70	3248	3583	26	−0.98
81	2998	2998	0.021935	0.000160	0.000665	0.000004	0.280893	0.000020	0.280990	−61.6	4.53	0.70	3068	3117	27	−0.98
82	2931	2931	0.035222	0.000112	0.001004	0.000007	0.280985	0.000018	0.280928	−63.2	0.77	0.66	3154	3306	25	−0.97
83	3002	3002	0.017100	0.000218	0.000565	0.000004	0.280970	0.000021	0.280937	−63.7	2.74	0.73	3138	3234	27	−0.98
86	2868	2868	0.054650	0.000341	0.001487	0.000008	0.281060	0.000022	0.280979	−60.5	1.09	0.77	3090	3237	30	−0.96
89	3064	3064	0.022600	0.000221	0.000982	0.000009	0.281438	0.000160	0.281380	−47.2	19.96	5.71	2536	2167	219	−0.97
91	2878	2878	0.026530	0.000227	0.000938	0.000006	0.280853	0.000051	0.280801	−67.9	−5.0	1.80	3326	3633	68	−0.97
95	2913	2913	0.024778	0.000605	0.000954	0.000019	0.281001	0.000037	0.280948	−62.6	1.04	1.32	3128	3275	50	−0.97
97	2766	2766	0.016612	0.000858	0.000573	0.000027	0.280977	0.000025	0.280946	−63.5	−2.42	0.89	3129	3383	33	−0.98
108	2888	2888	0.024835	0.000318	0.000977	0.000012	0.280844	0.000027	0.280790	−68.2	−5.16	0.97	3341	3650	37	−0.97
111	2961	2961	0.012159	0.000185	0.000503	0.000007	0.280872	0.000033	0.280843	−67.2	−1.56	1.18	3263	3477	44	−0.98
112	2765	2765	0.029870	0.000461	0.001074	0.000016	0.280994	0.000029	0.280938	−62.9	−2.76	1.03	3146	3404	39	−0.97
114	2961	2961	0.017560	0.000349	0.000617	0.000012	0.280974	0.000027	0.280939	−63.6	1.84	0.96	3137	3261	36	−0.98
115	2884	2884	0.022550	0.000410	0.000931	0.000018	0.280910	0.000035	0.280859	−65.9	−2.81	1.25	3248	3498	47	−0.97

[a] Spot numbers are the same as those of U—Pb dating.
[b] Initial $^{176}Hf/^{177}Hf$ ratio, calculated using crystallization age.
[c] $\varepsilon_{Hf}(t)$was calculated using crystallization age.
[d] Depleted mantle Hf two-stage model age calculated using crystallization age.
[e] Enrichment factor, defined as $(^{176}Lu/^{177}Hf)_{sample}/(^{176}Lu/^{177}Hf)_{CHUR}^{-1}$.

Table 4
Whole-rock major (wt%) and trace element (ppm) compositions of the Yangpo metapelites.

Sample	ZX02–3	ZX02–4	ZX02–5	ZX02–6	ZX02–7
Major element (wt%)					
SiO_2	62.20	62.62	60.49	64.27	62.31
Al_2O_3	15.56	15.30	18.12	16.65	15.68
CaO	2.08	2.18	1.66	2.49	1.59
Fe_2O_3	2.16	1.88	2.33	2.32	1.88
FeO	6.66	6.74	4.94	5.19	7.71
K_2O	1.04	1.02	2.37	1.50	1.66
MgO	4.82	5.06	4.84	3.28	4.14
MnO	0.11	0.09	0.07	0.11	0.12
Na_2O	0.59	0.77	0.93	0.88	0.46
P_2O_5	0.46	0.26	0.09	0.10	0.16
TiO_2	0.84	0.82	0.93	0.84	0.84
LOI	2.26	2.74	2.39	1.65	1.83
Total	96.52	96.74	96.77	97.63	96.55
Fe_2O_3t	9.04	8.81	7.50	7.74	9.78
K_2O/Na_2O	1.76	1.32	2.55	1.70	3.61
SiO_2/Al_2O_3	4.00	4.09	3.34	3.86	3.97
Al_2O_3/TiO_2	18.52	18.66	19.48	19.82	18.67
DF	−8.47	−8.38	−6.49	−5.76	−8.22
CIA	72.55	70.69	71.78	68.63	74.19
PIA	75.20	73.05	77.35	71.52	79.16
ICV	1.19	1.23	1.01	1.01	1.19
Trace element (ppm)					
Sc	22.30	20.10	29.10	26.0	28.20
Ti	7238.0	4033.0	1315.0	1628.0	2612.0
V	52.80	28.40	204.0	108.0	68.30
Cr	33.10	39.50	592.0	490.0	278.0
Co	15.60	13.0	45.90	28.70	27.20
Ni	25.10	23.20	258.0	148.0	119.0
Cu	358.0	140.0	66.70	38.0	202.0
Zn	170.0	210.0	165.0	161.0	222.0
Ga	25.70	27.0	24.30	24.0	25.80
Rb	45.10	45.0	98.40	60.70	74.50
Sr	111.0	129.0	173.0	212.0	75.70
Y	127.0	70.80	25.60	36.30	54.60
Zr	372.0	345.0	133.0	130.0	308.0
Nb	13.70	13.80	6.48	21.40	12.0
Cs	20.20	17.60	27.20	17.40	30.20
Ba	305.0	274.0	573.0	497.0	485.0
La	44.0	36.90	29.50	28.30	31.50
Ce	82.70	70.10	52.20	47.40	59.30
Pr	11.90	10.10	7.08	6.82	8.17
Nd	61.10	51.80	33.20	33.50	39.20
Sm	12.20	10.20	5.63	5.92	7.63
Eu	3.39	3.05	1.48	2.0	2.15
Gd	15.20	11.40	5.28	5.98	8.86
Tb	2.42	1.74	0.77	0.99	1.49
Dy	16.10	11.80	4.63	6.41	10.30
Ho	3.59	2.59	1.04	1.35	2.13
Er	10.70	7.99	2.95	3.94	6.12
Tm	1.70	1.29	0.46	0.62	0.94
Yb	10.70	8.46	3.0	4.10	6.03
Lu	1.67	1.27	0.44	0.60	0.91
Hf	10.30	9.74	4.81	4.58	8.49
Ta	1.19	1.11	0.64	1.65	1.14
Pb	14.0	16.0	19.7	21.8	14.4
Th	5.03	5.02	5.63	5.18	5.22
U	1.92	1.50	1.63	1.28	1.74
K/Rb	191.40	188.10	199.90	205.10	184.90
Rb/Sr	0.41	0.35	0.57	0.29	0.98
Th/Sc	0.23	0.25	0.19	0.20	0.19
Th/U	2.62	3.35	3.45	4.05	3.00
La/Co	2.82	2.84	0.64	0.99	1.16
Cr/Zr	0.09	0.11	4.45	3.77	0.90
Cr/Th	6.58	7.87	105.15	94.59	53.26
ΣREE	277.37	228.69	147.66	147.93	184.73
LREE/HREE	3.47	3.91	6.95	5.17	4.02
$(La/Yb)_N$	2.95	3.13	7.05	4.95	3.75
$(Gd/Yb)_N$	1.18	1.11	1.46	1.21	1.22
Eu/Eu*	0.76	0.86	0.83	1.03	0.80

DF = 10.44–0.21SiO_2–Fe_2O_3–0.98MgO + 0.55CaO + 1.46 Na2O + 0.54 K_2O (molar proportions), Shaw, 1972.
CIA = [Al_2O_3/(Al_2O_3 + CaO* + Na_2O + K_2O)]*100 (molar proportions), Nesbitt and Young, 1982.
ICV = (Fe_2O_3t + K_2O + Na_2O + CaO* + MgO + TiO_2)/Al_2O_3 (molar proportions), Cox et al., 1995.
(CaO* represents the CaO content in the silicate fraction. After correcting for P_2O_5, if the mole fraction of CaO ≤ Na_2O, then CaO* = CaO; if CaO ≥ Na_2O, then CaO* = Na_2O).
Eu/Eu* = $Eu_N/(Sm_N{}^*Gd_N)^{1/2}$.

TiO_2, and Al_2O_3 of the metapelites exhibit a general linear array when plotted against each other in the binary diagrams (Supplementary Fig. S1), further validating the immobility of these elements during chemical weathering (Fralick and Kronberg, 1997; Wang and Zhou, 2013).

5.2.2. Source weathering and post-depositional metasomatism

The chemical composition of clastic sediments is influenced by several geological factors related to sedimentary processes, such as source rock weathering and diagenesis (Cox et al., 1995; McLennan, 1989; McLennan et al., 1993). Weathering, as well as diagenesis, involves the conversion of unstable minerals, mainly feldspars and mica, to clay, and results in relative depletion of alkaline elements and LILEs, along with an enrichment of Al and Ti (Harnois, 1988; McLennan et al., 1993). The CIA (Chemical Index of Alteration) serves as a proxy for the intensity of chemical weathering and associated climate conditions (Fedo et al., 1997; Nesbitt and Young, 1982). The Yangpo metapelites have consistent CIA values between 68.63 and 74.19, which is comparable with the average Archean shale (CIA = 70.0–75.0; Nesbitt and Young, 1982), indicating mild chemical weathering in the source areas and, by inference, an overall cold or cold-dry paleoclimate (e.g.,Fedo et al., 1995; White and Blum, 1995; Yang et al., 2016). This is in agreement with the Th/U ratios of the metapelites (2.62–4.05) being mostly lower than the upper crust values (~4.0) (Fig. 9a), because otherwise a substantial increase of Th/U ratio would be expected as a result of oxidation and the loss of uranium during intense source weathering (McLennan et al., 1993; Partin et al., 2013).

Post-depositionalK-metasomatism is manifested either by conversion of clay minerals (e.g.,kaolinite as the matrix) to illite or conversion of plagioclase to K-feldspar(Fedo et al., 1995). On the ternary diagram (molecular proportion) of A-CN-K(Nesbitt and Young, 1989) (Fig. 9b), the metapelites show a trend roughly parallel to the CN-K join, indicating weak to moderate K-metasomatism by conversion of plagioclase to K-feldspar(Fedo et al., 1995; Wang and Zhou, 2013). This implies that the calculated CIA values for the metapelites have not significantly changed since the replacement of plagioclase by K-feldspar did not change the value of K_2O + Na_2O (Fedo et al., 1995). This interpretation is consistent with the CIA values of the metapelites being only slightly lower than the corresponding PIA (Plagioclase Index of Alteration; Fedo et al., 1995) values (71.52–79.16; Table 4). The quartz schist samples of Wang et al. (2013), however, are plotted along the A-K join and are markedly shifted from the weathering trend (Fig. 9b), which reflects relatively intense K-metasomatism by conversion of aluminous clay minerals to illite. The generally high PIA value (92.87–96.55; calculated from Wang et al. (2013a)) possibly indicates a higher degree of source weathering for the quartz schists than the metapelites. The more uniform and lower SiO_2/Al_2O_3 (3.34–4.09) and K_2O/Na_2O (1.32–3.61) ratios of the metapelites compared to the quartz schists (SiO_2/Al_2O_3 = 6.61–12.58, K_2O/Na_2O = 32.10–79.75; Wang et al., 2013a) further suggest less intense post-depositional silicification and K-metasomatism of the protoliths of the metapelites, relative to the quartz schists (Cullers et al., 1993). These observations indicate that primary geochemical signatures are better retained in the metapelites than quartz schists of the Yangpo "Group".

5.2.3. Sedimentary sorting

Sorting may influence the bulk chemical composition in that it may preferentially concentrate detrital heavy minerals. The Index of Compositional Variability (ICV), which measures the abundance of alumina

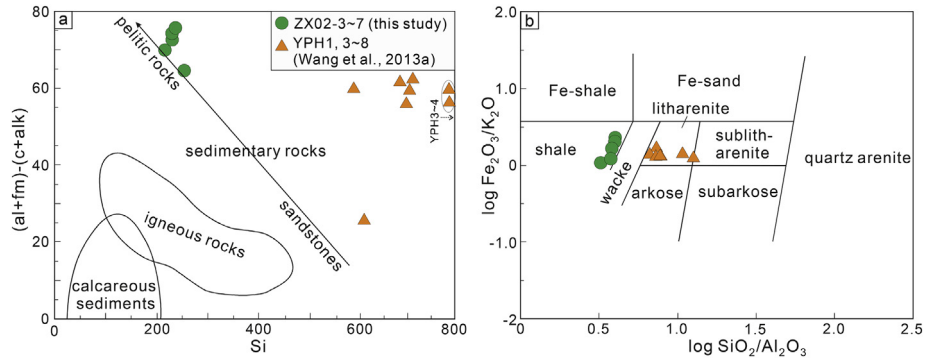

Fig. 7. Classification for metapelite samples from the Yangpo "Group" using (a)Niggli index discrimination diagram (Winkler, 1976) and (b)log (Fe_2O_3/K_2O) vs. log (SiO_2/Al_2O_3) plot (Herron, 1988). Data from quartz schist samples of the Yangpo "Group" (Wang et al., 2013a) are also plotted for comparison.

relative to other major cations in a host rock, is generally employed to evaluate the compositional maturity, and thus the degree of sorting (Cox et al., 1995). High ICV values of the Yangpo metapelites (1.01–1.23, average 1.12) indicate the deposition of compositionally immature first-cycle materials (Cox et al., 1995). Such compositional immaturity of the protoliths of the metapelites is also reflected in their low ratios of SiO_2/Al_2O_3 (3.34–4.09, average = 3.85) that are identical with the AUCC values (average = 3.93; Taylor and McLennan, 1985). On the Th/Sc vs. Zr/Sc diagram (McLennan et al., 1993) (Fig. 9c), the metapelite samples displace towards low Zr/Sc ratios (<10) and appear to be shifted from the compositional variation trend, indicating relatively low degrees of sediment recycling and sorting; the chemical immaturity of the Yangpo metapelites also contrasts with the quartz schists, which have relatively low ICV values (0.67–0.83, average 0.72; calculated from Wang et al. (2013a)).

5.2.4. Nature of source rocks

Generally, the SiO_2/Al_2O_3 ratio increases when sediments are transported from the source area to a sedimentary basin, rendering this parameter usually lower in the source rocks than in the sediments (McLennan et al., 1993). In the case of insufficient local outcrops, a simple chemical comparison of the studied metapelites with the global average of Archean rock may help discriminate source rock characteristics (Wang et al., 2017). The Yangpo metapelites have SiO_2/Al_2O_3 ratios (3.34–4.09, average 3.85) that are identical or slightly higher than the end member ratio of average Archean mafic component (3.40; Taylor and McLennan, 1985), indicating an important contribution from mafic source rocks. However, among the studied samples, the maximum SiO_2/Al_2O_3 ratio is 4.09, close to the end member ratio of Archean felsic component (4.41; Taylor and McLennan, 1985) and of the potential source rocks in the Zhongxiang Complex (4.54, trondhjemitic gneisses; see below), suggesting that felsic rocks also contributed to the sedimentary source of the metapelites. In contrast, calculated SiO_2/Al_2O_3 ratios (6.61–12.58, average 8.58) of the quartz schist samples of Wang et al. (2013a)appear to be much higher than the end member ratio of Archean felsic component, which could be attributed either to an extremely high proportion of felsic component in their source or the relatively intense post-depositional silicification and K-metasomatism of the protoliths, as discussed above.

On the A-CN-K diagram (Fig. 9b), the array of the Yangpo metapelites intersects the A-CN boundary at positions corresponding to the compositional spectrum among basalt, andesite, and granodiorite (Fig. 9b). Because it is commonly recognized that the Archean upper continental crust was dominated by basaltic and felsic rocks with only minor andesites (Taylor and McLennan, 1995), and Archean andesites are yet not documented in the Yangtze Craton, a mixed source comprising granodioritic and basaltic rocks is more plausible for the protoliths of the studied metapelites. Such mixed source nature is consistent with the Th/Sc vs. Zr/Sc, Co/Th vs. La/Sc, and La/Th vs. Hf plots (Condie, 1993; McLennan et al., 1993), which show transitional source compositions between mafic and felsic source components (Fig. 9c–e). Chemical compositions of the quartz schist samples of Wang et al. (2013a), by contrast, indicate a source with possibly more felsic rocks and less mafic rocks compared to the metapelites (Fig. 9b–e).

Archean andesites are absent in the Yangtze Craton. Following Condie (1993) and Gao and Wedepohl (1995), we carried out a three-component mixing calculation using the REE systematics of average Archean TTG and granites available from the Zhongxiang Complex, which possibly provided the main detritus (see below; Wang et al., 2018), and

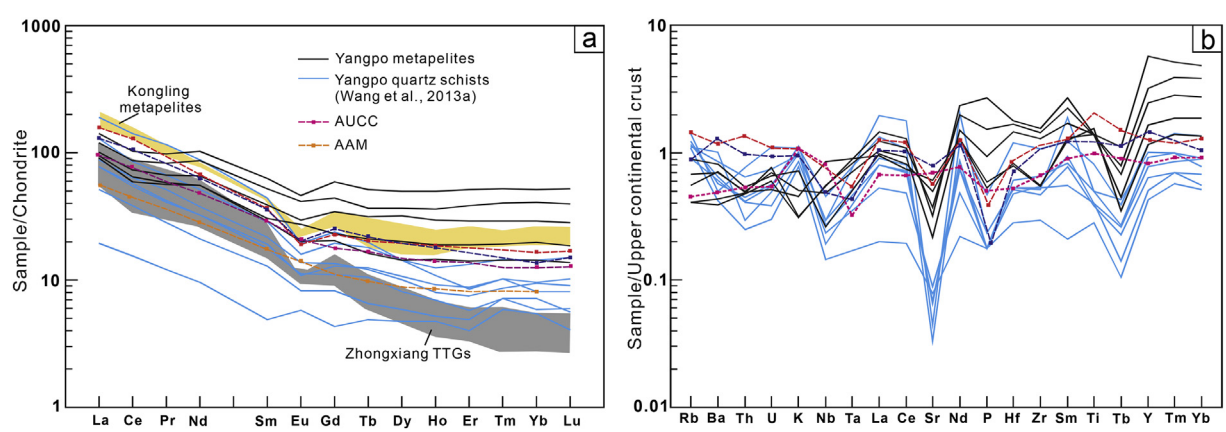

Fig. 8. (a)Chondrite-normalized REE patterns and (b)Upper continental crust-normalized multiple trace element diagrams of metapelite samples from the Yangpo "Group". Quartz schist samples from the Yangpo "Group" (Wang et al., 2013a) are also plotted for comparison. Chondrite normalizing values are from Boynton (1984) and those of the upper continental crust are from Taylor and McLennan (1985). The standard composition of Archean Upper Continental Crust (AUCC) after Taylor and McLennan (1995), and Archean Average Mudstone (AAM) after Taylor and McLennan (1985) are shown for comparison. Data of Zhongxiang TTGs and Kongling metapelites are from Wang et al. (2018) and Li et al. (2016), respectively.

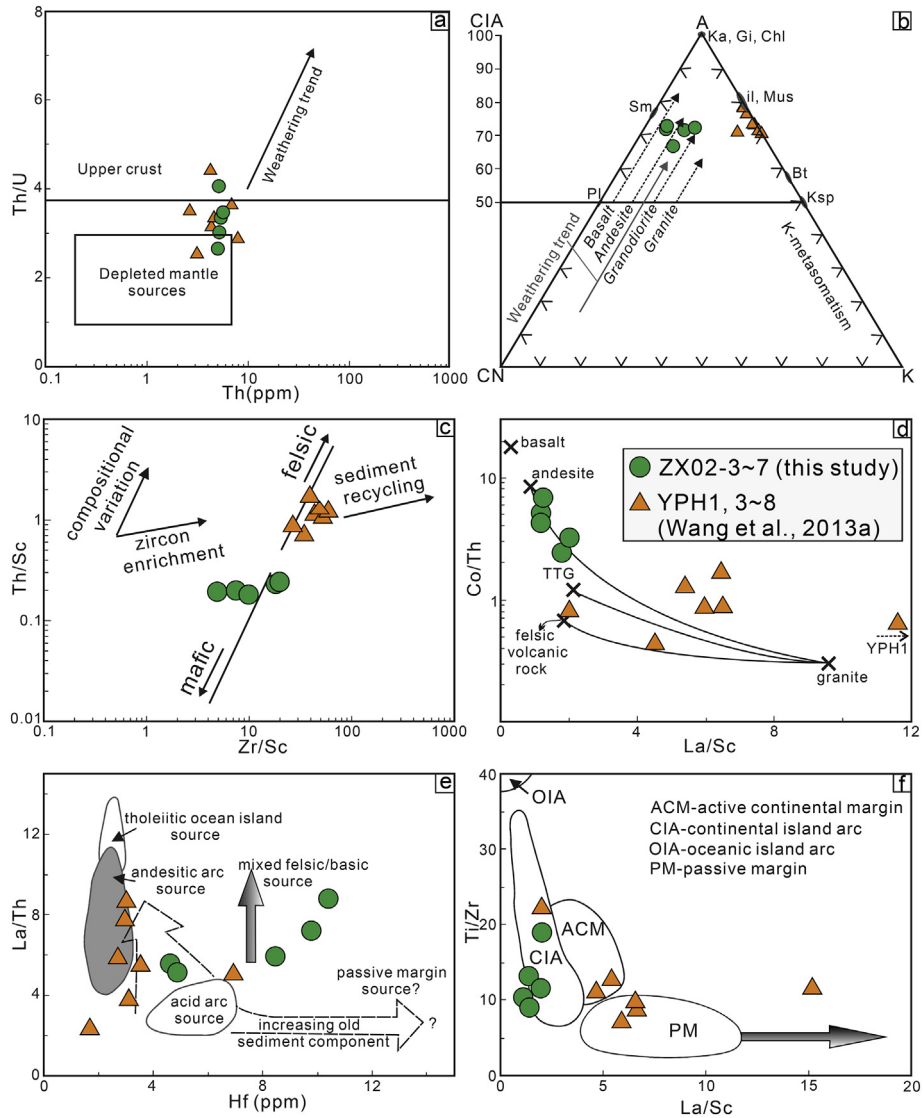

Fig. 9. Geochemical diagrams for the Yangpo metapelites. (a)Plot of Th/U ratios vs. Th abundances (McLennan et al., 1993). (b)Ternary plot of molecular proportions Al_2O_3(A)—CaO + Na_2O (CN)—K_2O(K)(Nesbitt and Young, 1989) with Chemical Index of Alteration (CIA) scale. Also shown are idealized mineral and magmatic rock compositions: Ka = kaolinite, Gi = gibbsite, Chl= chlorite, Il = illite, Mus = muscovite, Bt = biotite, Ksp = K-feldspar, Sm = smectite, Pl = plagioclase. Dashed black arrows represent weathering trends of different magmatic rocks. (c)Th/Sc-Zr/Sc diagram (McLennan, 1993). (d)Co/Th vs. La/Sc diagram. Average compositions of references are from Condie (1993). (e)La/Th vs. Hf diagram (Floyd and Leveridge, 1987). (f)Ti/Zr vs. La/Sc diagram (Bhatia and Crook, 1986). Data from quartz schist samples of the Yangpo "Group" (Wang et al., 2013a) are also plotted for comparison.

of the global average of a basalt-komatiite mixture (Condie, 1993); the TTG and granite REE compositions of the supposed source rocks are comparable with the average data of their global lithologic counterparts (Table 5; Condie, 1993). It indicates that no >30% granitic rock is expected to have been involved in the detritus of the protoliths of the Yangpo metapelites with Eu/Eu* value of 0.86, and that >60% basalt-komatiite mixture is needed to generate a $(La/Yb)_N$ value of 4.40 in the derived mixtures, which is dissimilar to the source with >65% felsic component (granite+TTG) expected for the protoliths of the quartz schists. Collectively, we infer that the protoliths of the Yangpo metapelites were sourced from first-cycle erosion products of both mafic and felsic rocks, with mafic rocks possibly accounting for a relatively higher proportion than felsic rocks.

5.2.5. Possible depositional setting

On the Ti/Zr vs. La/Sc diagram (Fig. 9f), the metapelites cluster within the field of continental island arc, whereas the quartz schists are plotted within both the field of passive margin and the field of active continental margin. This is, however, different from the geochemical discriminations involving some mobile oxides of the quartz schists (Wang et al., 2013a), which indicate a deposition of the protoliths of the quartz schists in a relatively stable tectonic setting. While there is limited geologic constraint from the Zhongxiang Complex and adjacent area, the abovementioned 2.67–2.62 Ga A_2-type granites in the northern Zhongxiang Complex, which emplaced immediately following the deposition of the Yangpo "Group", may herald the onset of late-collisional crustal extension related to the collapse of orogenic roots in the Zhongxiang Complex area (Wang et al., 2013a, 2013b; Wang et al., 2018; Zhou et al., 2015). The 2.70–2.67 Ga Yangpo metapelites that predate the late-collisional event are thus speculated to have been deposited in a basin near an active continental margin. This interpretation is consistent with the lack of significant Eu anomalies and flat REE patterns (Fig. 8a), and the chemical immaturity of the protoliths of the Yangpo metapelites. Nevertheless, we acknowledge that the tectonic setting for the Archean sedimentation is still a matter of debate due to the scarcity of geologic records available, and the likely different thermal regime compared to the post-Archean time (McLennan and Taylor, 1991).

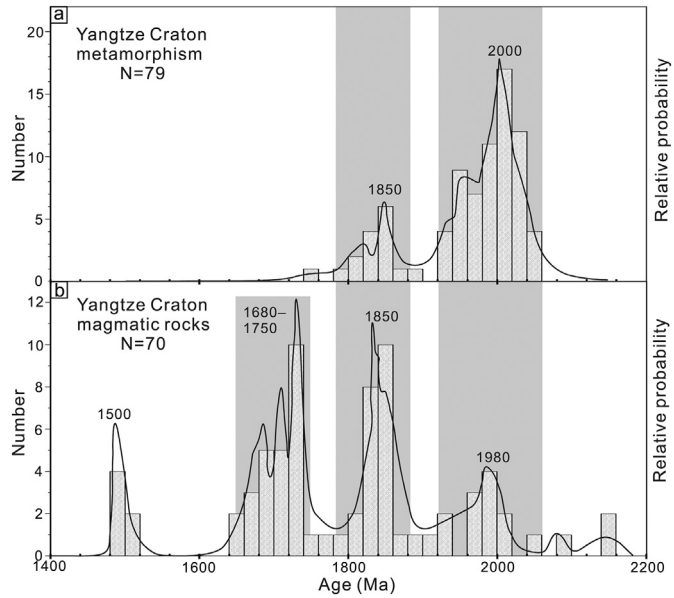

Fig. 10. Relative histograms and probability plots of late Paleoproterozoic to Mesoproterozoic (2.2–1.4 Ga) (a)metamorphic and (b)magmatic ages from the Yangtze Craton. N = number of the U—Pb dating sample used in each compilation. The metamorphic age obtained in this study is also included, and others are compiled in Supplementary TableS1, where corresponding lithologies, analytical methods, and references are listed.

5.3. Zircon-based provenance

A standard practice in provenance studies of a sedimentary rock is to compare its detrital zircon age and Hf isotopic signatures with those of possible source regions (Gehrels, 2014). Given the immature geochemical compositions of the metapelites, we consider the local Archean crustal units of the Yangtze Craton as the most likely detrital provenance(s).

The largest detrital zircon clusters from the metapelite samples are 2.92–2.85 Ga and 2.80–2.73 Ga in age, which show two prominent age peaks at 2.87 Ga and 2.78 Ga, respectively (Fig. 5c, d). This suggests that the detritus were derived from a provenance dominated by 2.87 Ga and 2.78 Ga rocks. Zircon grains for both age groups are mostly euhedral to subhedral with clear oscillatory zoning (Fig. 4), implying that their primary sources were not far from the site of deposition. Zircons within individual groups, however, show contrasting Hf isotopic compositions, with the older and younger groups yielding predominantly positive and negative $\varepsilon_{Hf}(t)$values, respectively (Fig. 11). Trondhjemitic gneisses, granites, and amphibolites of the Kongling Complex that are 2.90 Ga, 2.86 Ga, and 2.80–2.78 Ga in age, respectively (e.g., Wu et al., 2009; Chen et al., 2013a; Guo et al., 2015; Table 1), were possible source rocks providing the 2.92–2.85 Ga and 2.80–2.73 Ga detrital zircons to the Yangpo metapelites. However, these magmatic rocks have 2.90 and 2.86 Ga magmatic zircons with highly variable and mostly negative $\varepsilon_{Hf}(t)$values, and 2.80–2.78 Ga magmatic zircons that have exclusively negative $\varepsilon_{Hf}(t)$values, both of which are very different from similar-aged detrital zircons in the Yangpo metapelites (Fig. 11). Such isotopic contrasts do not necessarily preclude the Kongling Complex from being a contributing source, but render it unlikely a major source for the dominantly 2.92–2.85 Ga and 2.80–2.73 Ga detrital zircons in the Yangpo metapelites. In contrast, the recently documented granitic rocks in the southern Zhongxiang Complex, dated at 2.90–2.87 Ga and 2.77 Ga (Wang et al., 2018), could be the primary zircon provenance. Magmatic zircons from these rocks have $\varepsilon_{Hf}(t)$values that totally or partially overlap with those of similar-aged detrital zircons in the Yangpo metapelites (Fig. 11). Thus, the Zhongxiang Complex itself was capable of feeding the Neoarchean basin, in which the protoliths of the Yangpo metapelites accumulated.

The oldest zircons with a relatively minor contribution to the Yangpo metapelites are 3.0 Ga in age. Rocks of this age are yet to be reported from the Yangtze Craton, but slightly younger magmatic rocks (2951 ± 20 Ma, granodioritic gneisses; Gao et al., 2011) have been identified from the Kongling Complex. However, these granodioritic gneisses possess highly variable zircon $\varepsilon_{Hf}(t)$values from strongly negative to positive, which are inconsistent with the similar-aged detrital zircons with generally positive $\varepsilon_{Hf}(t)$values in the Yangpo metapelites (Fig. 11). Meanwhile, 2.70 Ga magmatic rocks are absent in the Zhongxiang Complex but are preserved in the Kongling Complex (granitic gneisses; Chen et al., 2013a) and the Yudongzi Complex (granites; Zhang et al., 2010) (Table 1). Zircons from these 2.70 Ga magmatic rocks differ from similar-aged detrital zircons in the Yangpo metapelites in that they have more depleted Hf-isotope compositions (Fig. 11). Also noteworthy is that the predominant Paleoarchean ages (3.45–3.20 Ga; Table 1) of TTG gneisses within the Kongling Complex, which are absent in our detrital zircon records. Therefore, Archean crustal provinces outside the Zhongxiang Complex, generally with different age and Hf isotopic compositions (Wang et al., 2018), are supposed to be less important contributors to the 3.0 Ga and 2.70 Ga detrital zircons in the Yangpo metapelites. The likelihood that the Kongling Complex provided detritus to the Neoarchean Yangpo metapelites is further overshadowed by the recent documented Paleoproterozoic NE-SW trending ophiolitic mélange in the Kongling Complex, which is interpreted to be a tectonic suture between the proposed eastern and western micro-continents in the Yangtze Craton (Han et al., 2017). If correct, it is unlikely that the Kongling Complex shed detritus on the Yangpo metapelites of the Zhongxiang Complex, another possible independent crustal unit prior to the Archean (Wang et al., 2018; see discussion in Section 5.5). The subangular to subrounded external habits and prismatic shapes of many 3.0 Ga and 2.70 Ga detrital zircons from the metapelite samples suggest a short sedimentary transport distance, favoring the unknown local rocks within the Zhongxiang Complex to be the source region.

Collectively, detrital zircon age and Hf-isotope data from the Yangpo metapelites indicate local zircon provenances mainly within the Zhongxiang Complex. We consider pre-2.70 Ga rocks of the Zhongxiang Complex as the principal source providing the bulk detritus for the Yangpo metapelites, although currently known pre-2.70 Ga rocks in the Zhongxiang Complex are all felsic in composition, differing from the mixed (ultra)-mafic and felsic signature expected of the source rocks of the Yangpo metapelites (see above). We therefore suggest that the source rocks for the Archean Yangpo metapelites, especially the source provided the (ultra)-mafic components, are either currently concealed in the region, or they have been largely eroded during or after the deposition of the Yangpo "Group".

5.4. Archean crustal evolution of the Zhongxiang Complex

Detrital zircon age data from the Yangpo metapelites imply that the source regions had major magmatic episodes of 3.0 Ga, 2.92–2.85 Ga, 2.82–2.73 Ga, and 2.70 Ga, suggesting crustal generation and/or reworking events at these time periods. The 3.0 Ga zircons generally have positive $\varepsilon_{Hf}(t)$values (Fig. 11; Table 3), implying possibly significant juvenile crustal growth in the middle Mesoarchean. A much larger group of detrital zircon grains in our samples is 2.92–2.85 Ga in age and we have interpreted a likely source from locally exposed rocks in the Zhongxiang Complex, which is represented by the 2.90–2.87 Ga Huachong granites (Wang et al., 2018). Whilst possible reworking of the older crust is also associated with extraction of juvenile materials in the genesis of the Huachong granites, the preponderance of magmatic zircons yielding negative $\varepsilon_{Hf}(t)$values would imply dominant inputs of reworked crust (Fig. 11). Data from our detrital zircons would further suggest that this magmatic episode has also involved a significant input of juvenile materials, as some of the detrital zircon grains

Table 5
Average trace elemental abundances and ratios of Yangpo metapelite samples used in mixing calculations, compared to those of average Archean (ultra)-basic rock, granite, TTG, shale, and end-member mixtures, and potential source rocks in the Zhongxiang Complex.

	BK mixture	Granite	TTG	Shale	MIX-A	MIX-B	MIX-C	ZX granite	ZX TTG	Yangpo quartz schist	Yangpo metapelite
SiO_2	50.10	72.40	69.50	61.0	64.0	59.0	61.0	77.50	71.1	81.49	62.41
MgO	11.90	0.40	1.10	3.90	4.60	7.30	6.20	0.25	0.61	0.68	4.57
Cr	790.0	16.0	22.0	507.0	288.0	480.0	404.0	2.60	3.30	78.51	286.52
Th	0.90	15.0	8.0	8.50	8.70	6.50	7.30	16.30	14.60	4.83	5.22
V	228.0	15.0	37.0	154.0	94.0	143.0	124.0	4.90	14.10	31.34	92.30
Sc	35.0	4.0	5.0	21.0	15.0	23.0	20.0	3.30	3.70	4.16	25.14
FeOt	10.20	1.90	3.5	7.50	5.10	6.90	6.20	1.30	1.40		8.42
Zr	75.0	155.0	160.0	151.0	128.0	107.0	116.0	215.50	99.10	140.0	257.60
Y	18.0	20.0	13.0	28.0	18.0	19.0	18.0	19.70	6.50	17.10	62.86
La	6.50	50.0	30.0	31.0	30.80	23.90	26.30	41.0	17.80	27.85	34.04
Nd	9.60	46.0	22.0	27.70	28.50	2.20	25.40	34.30	16.60	23.35	43.76
Sm	2.64	6.30	3.40	4.85	4.0	4.10	4.18	5.60	2.60	4.13	8.32
Yb	2.10	2.0	1.0	2.40	1.80	2.06	1.95	2.88	0.56	1.79	6.46
Eu/Eu*	0.99	0.48	0.97	0.73	0.76	0.78	0.78	0.54	0.86	0.80	0.86
$(La/Yb)_N$	1.90	15.20	18.20	7.80	10.20	7.0	8.20	14.0	26.70	11.06	4.37
Cr/Th	878.0	1.10	2.80	60.0	33.0	73.0	56.0	0.16	0.23	16.29	53.49
Th/Sc	0.03	3.75	1.60	0.40	0.58	0.29	0.37	4.94	3.95	1.15	0.21
Zr/Y	4.20	7.80	12.30	5.40	7.20	5.70	6.30	10.90	15.20	8.29	4.44
Sm/Nd	0.28	0.14	0.16	0.175	0.16	0.17	0.17	0.16	0.16	0.18	0.19

Basalt-komatiite mixture ratio is 85:15. Average rock compositions of Archean basalt, komatiite, granite, TTG, and shale are from Condie (1993), and of the Zhongxiang Archean TTG andgranite are from our unpublished data. Mixture A: BK: GR: TTG = 35: 45: 20; Mixture B: BK: GR = 60: 40; Mixture C: BK: GR: TTG = 50: 40: 10. BK = basalt-komatiite mixture; GR = granite; TTG = tonalite-trondhjemite-granodiorite. ZX–the Zhongxiang Complex.

have depleted Hf-isotope compositions (Fig. 11). Meanwhile, the 2.82–2.73 Ga zircon group has restricted Hf isotopic compositions with predominantly negative $\varepsilon_{Hf}(t)$values (Fig. 11). Such Hf-isotope signatures are in good agreement with those of the 2.77 Ga magmatic zircons in the Youjiangchong trondhjemitic gneisses (Wang et al., 2018) (Fig. 11), which together suggest that the magmatic episode of 2.82–2.73 Ga involved mainly the reworking of ancient crust in the Zhongxiang Complex. In addition, the small zircon group with ages between 2.73 and 2.68 Ga, generally with negative $\varepsilon_{Hf}(t)$values (Fig. 11), represents another Neoarchean magmatic event that possibly involved the reworking of the Zhongxiang crust.

It is noted that a majority of the detrital zircons converge towards important contributions from older continental crustal materials (Fig. 11), indicating the existence of enough continental crust that had formed in the early Archean to be registered in the sedimentary provenance. Generally, T_{DM}^{C} ages do not represent the time of crust-mantle differentiation, but an estimate of the average crustal residence time of multiple sources (Hawkesworth et al., 2010). However, through compilations of a large dataset, important constraints can still be placed on the timing of the upper continental crust (Wang et al., 2012b). The T_{DM}^{C} ages of detrital zircons from the Yangpo metapelites are contrasted against those of the Archean magmatic zircons from different Archean crustal provinces of the Yangtze Craton (Fig. 12). It can be seen that the detrital zircons are dominated by a subordinate T_{DM}^{C} age population of 3.55–3.45 Ga (peak at 3.50 Ga) and a major population of 3.40–3.25 Ga (peak at 3.30 Ga), which compares well with the T_{DM}^{C} age pattern of the Archean magmatic zircons from the Zhongxiang Complex, providing evidence for two major episodes of possible crustal growth during these time periods in the Zhongxiang Complex.

To summarize, the Archean continental crust of the Zhongxiang Complex was likely built through early crustal growth at 3.55–3.45 Ga and 3.40–3.0 Ga, followed by continuous extraction of juvenile materials accompanied by reworking of ancient crust at 2.92–2.85 Ga, and significant crustal reworking events at 2.80–2.70 Ga and 2.67–2.62 Ga.

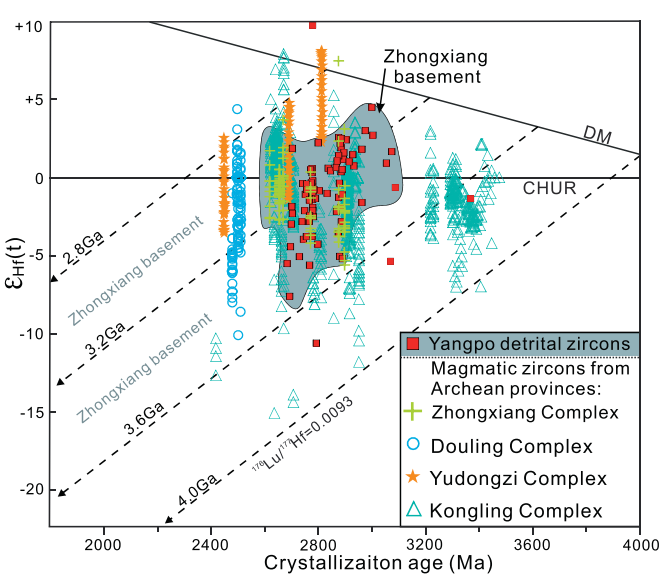

Fig. 11. Zircon $\varepsilon_{Hf}(t)$versus crystallization age plot of detrital zircons from the Yangpo metapelites. Magmatic zircon data from Archean magmatic rocks in the Kongling, Zhongxiang, Douling, and Yudongzi complexes are shown for comparison. See Table 1 for data sources.

5.5. Implications for early evolution of the Yangtze Craton

It is commonly believed that a greater number of potentially independent microcontinents or terranes existed with progressively older geologic times (Evans, 2013). The Yangtze Craton, which features a prolonged crustal growth history between 3.45 and 2.50 Ga (e.g.,Guo et al., 2014, 2015), has been interpreted either as a single uniform continental block (Wang et al., 2015; Zhou et al., 2015) or a collage of several distinct blocks (Wu et al., 2012; Zhang and Zheng, 2013; Li et al., 2016; Hui et al., 2017). Besides the Zhongxiang Complex, as shown above, several other Archean crustal provinces including the Kongling Complex, the Yudongzi Complex, the Douling Complex, the Huangtuling granulites, and the Phan Si Pan Complex have been documented in the Yangtze Craton. A preliminary synthesis of the existing age and chemical data of the Archean magmatic rocks demonstrated considerable differences in the magmatic histories among these crustal provinces (Table 1; Wang et al., 2018). Our updated interpretation of the Archean Zhongxiang Complex, as discussed above, further shows distinguishable crustal compositions between the Zhongxiang Complex and other Archean provinces (Figs.11 and 12), possibly reflecting varied Archean crustal evolution across the Yangtze Craton.

Archean crustal evolution recorded in ancient metasedimentary rocks also provides important information for deciphering the early

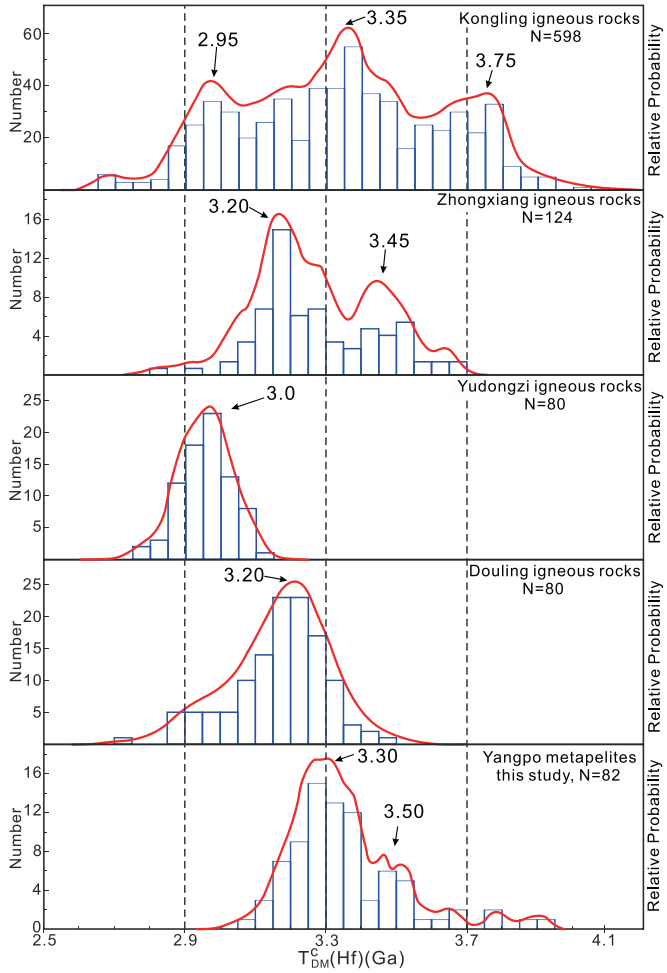

Fig. 12. Crustal Hf model age histograms and probability plots of detrital zircons from the Yangpo metapelites. Magmatic zircon data from Archean magmatic rocks in the Kongling, Zhongxiang, Douling, and Yudongzi complexes are shown for comparison. N = number Hf isotopic analysis. Data are compiled in Table 1.

history of the Yangtze Craton. The Yangpo "Group" documented in this study, as part of the Zhongxiang Complex, is the only confirmed Archean sedimentary unit in the Yangtze Craton. Detrital zircons in this study indicate inputs of mainly 2.87 Ga and 2.78 Ga crustal materials for the Yangpo metapelites, which is different from that documented in the 2.70–2.0 Ga Huangtuling granulites (mainly 2.70 Ga detrital zircons; Sun et al., 2008), indicating dissimilar sources for the two sedimentary units. Chemical data for the Huangtuling granulites and another potential Archean sedimentary unit in the Yudongzi Complex are yet unavailable. The Zhongxiang Complex therefore possibly underwent independent magmatic and sedimentary processes compared to other provinces of the Yangtze Craton during the Archean, hence supporting the multiple early terranes hypothesis for the origin of the Yangtze Craton.

6. Conclusions

We draw the following conclusions based on our new results and regional synthesis:

(1) The protoliths of metapelites of the Yangpo "Group", Zhongxiang Complex, were deposited during 2.70–2.67 Ga and metamorphosed at 1.95 Ga.
(2) The source rocks for the Yangpo metapelites were subjected to relatively weak chemical weathering and a low degree of physical sorting, with weak to moderate post-depositional silicification and K-metasomatism. The protoliths of the metapelites are compositionally immature, with a mixture of (ultra)-mafic rocks and felsic rocks in their source materials.
(3) The good agreement between age spectra and Hf isotopic characteristics of the detrital zircons in the Yangpo metapelites and those of the nearby magmatic rocks indicates that proximal older rocks within the Zhongxiang Complex were likely the main detrital source for the Yangpo metapelites.
(4) Zircon age and Hf isotopic data from this and previous studies together suggest that the Archean continental crust of the Zhongxiang Complex was likely built through three major episodes of possible crustal growth at 3.55–3.45 Ga, 3.40–3.0 Ga, and 2.92–2.85 Ga, followed by two major episodes of possible crustal reworking at 2.80–2.70 Ga and 2.67–2.62 Ga.
(5) The Yangtze Craton is likely a collage of multiple early terranes with a complex Archean crustal evolutionary history.

Supplementary data to this article can be found online at https://doi.org/10.1016/j.lithos.2018.09.027.

Acknowledgements

We thank editor Marco Scambelluri and three anonymous reviewers for constructive critiques that improved the accuracy and clarity of the manuscript. Critical suggestions and proofreading by Prof. William J. Collins, Dr. Rongfeng Ge, Adam R. Nordsvan, and Hamed Gamal El Dien greatly improved the early version of this paper. The assistance of Dr. Jianjun Cui, Yilong Xu, and Tao Zheng in fieldwork and U—Pb age analysis is much appreciated. This research was supported by research grants from China Geological Survey (CGS), China (Nos. 121201104000160916 and DD20179353), National Key R&D Plan of China (No. 2017YFC0601402), and the Australian Research Council Laureate Fellowship grant to Zheng-Xiang Li (FL150100133). This is a contribution to IGCP 648.

References

Ames, L., Zhou, G.Z., Xiong, B.C., 1996. Geochronology and isotopic character of ultrahigh-pressure metamorphism with implications for collision of Sino-Korean and Yangtze cratons, central China. Tectonics 15, 472–489.
Bhatia, M.R., Crook, K.A.W., 1986. Trace element characteristics of graywackes and tectonic setting discrimination of sedimentary basins. Contrib. Mineral. Petrol. 92, 181–193.
Blichert-Toft, J., Albarède, F., 1997. The Lu-Hf isotope geochemistry of chondrites and the evolution of the mantle-crust system. Earth Planet. Sci. Lett. 148, 243–258.
Bolhar, R., Kamber, B.S., Moorbath, S., Whitehouse, M.J., Collerson, K.D., 2005. Chemical characterization of earth's most ancient clastic metasediments from the Isua Greenstone Belt, southern West Greenland. Geochim. Cosmochim. Acta 69 (6), 1555–1573.
Bolhar, R., Hofmann, A., Siahi, M., Feng, Y.X., Delvigne, C., 2015. A trace element and Pb isotopic investigation into the provenance and deposition of stromatolitic carbonates, ironstones and associated shales of the ~3.0Ga Pongola Supergroup, Kaapvaal Craton. Geochim. Cosmochim. Acta 158, 57–78.
Boynton, W.V., 1984. Geochemistry of rare earth elements: meteorite studies. In: Henderson, P. (Ed.), Rare Earth Element Geochemistry. Elsevier, Amsterdam, pp. 63–114.
Bureau of Geology and Mineral Resources of Hubei Province (BGMRHP), 1990. Regional Geology of Hubei Province. Geological Publishing House, Beijing (in Chinese).
Chen, J.F., Foland, K.A., Xing, F.M., Xu, X., Zhou, T.X., 1991. Magmatism along the southeast margin of the Yangtze block: Precambrian collision of the Yangtze and Cathaysia blocks of China. Geology 19 (8), 815–818.
Chen, K., Gao, S., Wu, Y.B., Guo, J.L., Hu, Z.C., Liu, Y.S., Zong, K.Q., Liang, Z.W., Geng, X.L., 2013a. 2.6–2.7Ga crustal growth in Yangtze craton, South China. Precambrian Res. 224, 472–490.
Chen, W.T., Zhou, M.F., Zhao, X.F., 2013b. Late Paleoproterozoic sedimentary and mafic rocks in the Hekou area, SWChina: implication for the reconstruction of the Yangtze block in Columbia. Precambrian Res. 231 (5), 61–77.
Condie, K.C., 1993. Chemical composition and evolution of the upper continental crust: Contrasting results from surface samples and shales. Chem. Geol. 104, 1–37.
Cox, R., Lowe, D.R., Cullers, R.L., 1995. The influence of sediment recycling and basement composition on evolution of mudrock chemistry in the southwestern United States. Geochim. Cosmochim. Acta 59, 2919–2940.
Cullers, R.L., DiMarco, M.J., Lowe, D.R., Stone, J., 1993. Geochemistry of a silicified, felsic volcaniclastic suite from the early Archaean Panorama Formation, Pilbara Block, Western Australia: an evaluation of depositional and post-depositional processes

with special emphasis on the rare-earth elements. Precambrian Res. 60 (1–4), 99–116.
Dong, Y.P., Santosh, M., 2016. Tectonic architecture and multiple orogeny of the Qinling Orogenic Belt, Central China. Gondwana Res. 29 (1), 1–40.
Evans, D.A., 2013. Reconstructing pre-Pangean supercontinents. Geol. Soc. Am. Bull. 125 (11–12), 1735–1751.
Evans, D.A.D., Li, Z.X., Murphy, J.B., 2016. Four-dimensional context of Earth's supercontinents. In Li, Z.X., et al. (Eds.), Supercontinent cycles through Earth history. Geol. Soc. Lond., Spec. Publ. 424 (1), 1–14.
Fedo, C.M., Nesbitt, H.W., Young, G.M., 1995. Unraveling the effects of potassium metasomatism in sedimentary rocks and paleosols, with implications for paleoweathering conditions and provenance. Geology 23, 921–924.
Fedo, C.M., Young, G.M., Nesbitt, H.W., 1997. Paleoclimatic control on the composition of the Paleoproterozoic Serpent Formation, Huronian Supergroup, Canada: a greenhouse to icehouse transition. Precambrian Res. 86 (3–4), 201–223.
Fedo, C.M., Sircombe, K.N., Rainbird, R.H., 2003. Detrital zircon analysis of the sedimentary record. Rev. Mineral. Geochem. 53 (1), 277–303.
Floyd, P.A., Leveridge, B.E., 1987. Tectonic environment of the Devonian Gramscatho basin, south Cornwall: framework mode and geochemical evidence from turbiditic sandstones. J. Geol. Soc. 144, 531–542.
Fralick, P.W., Kronberg, B.I., 1997. Geochemical discrimination of clastic sedimentary rock sources. Sediment. Geol. 113 (1–2), 111–124.
Gao, S., Wedepohl, K.H., 1995. The negative Eu anomaly in Archean sedimentary rocks: implications for decomposition, age and importance of their granitic sources. Earth Planet. Sci. Lett. 133 (1–2), 81–94.
Gao, S., Ling, W.L., Qiu, Y.M., Lian, Z., Hartmann, G., Simon, K., 1999. Contrasting geochemical and Sm-Nd isotopic compositions of Archean metasediments from the Kongling high-grade terrain of the Yangtze craton: evidence for cratonic evolution and redistribution of REE during crustal anatexis. Geochim. Cosmochim. Acta 63 (13), 2071–2088.
Gao, S., Yang, J., Zhou, L., Li, M., Hu, Z.C., Guo, J.L., Yuan, H.L., Gong, H.J., Xiao, G.Q., Wei, J.Q., 2011. Age and growth of the Archean Kongling terrain, South China, with emphasis on 3.3Ga granitoid gneisses. Am. J. Sci. 311, 153–182.
Garçon, M., Carlson, R.W., Shirey, S.B., Arndt, N.T., Horan, M.F., Mock, T.D., 2017. Erosion of Archean continents: the Sm-Nd and Lu-Hf isotopic record of Barberton sedimentary rocks. Geochim. Cosmochim. Acta 206, 216–235.
Ge, R.F., Zhu, W.B., Wilde, S.A., He, J.W., Cui, X., Wang, X., Zheng, B.H., 2014. Neoproterozoic to Paleozoic long-lived accretionary orogeny in the northern Tarim Craton. Tectonics 33, 302–329.
Gehrels, G., 2012. Detrital zircon U-Pb geochronology: current methods and new opportunities. Tectonics Sediment. Basins Recent Advances 45–62.
Gehrels, G., 2014. Detrital zircon U-Pb geochronology applied to tectonics. Annu. Rev. Earth Planet. Sci. 42, 127–149.
Ghosh, S., Sarkar, S., 2010. Geochemistry of Permo-Triassic mudstone of the Satpura Gondwana basin, central India: clues for provenance. Chem. Geol. 277 (1–2), 78–100.
Greentree, M.R., Li, Z.X., 2008. The oldest known rocks in southwestern China: SHRIMPU-Pb magmatic crystallisation age and detrital provenance analysis of the Paleoproterozoic Dahongshan Group. J. Asian Earth Sci. 33 (5–6), 289–302.
Griffin, W.L., Wang, X., Jackson, S.E., Pearson, N.J., O'Reilly, S.Y., Xu, X.S., Zhou, X.M., 2002. Zircon chemistry and magma mixing, SEChina: in-situ analysis of Hf isotopes, Tonglu and Pingtan igneous complexes. Lithos 61, 237–269.
Guo, J.L., Gao, S., Wu, Y.B., Li, M., Chen, K., Hu, Z.C., Liang, Z.W., Liu, Y.S., Zhou, L., Zong, K.Q., Zhang, W., Chen, H.H., 2014. 3.45Ga granitic gneisses from the Yangtze Craton, South China: implications for early Archean crustal growth. Precambrian Res. 242, 82–95.
Guo, J.L., Wu, Y.B., Gao, S., Jin, Z.M., Zong, K.Q., Hu, Z.C., Chen, K., Chen, H.H., Liu, Y.S., 2015. Episodic Paleoarchean-Paleoproterozoic (3.3–2.0 Ga) granitoid magmatism in Yangtze craton, South China: implications for late Archean tectonics. Precambrian Res. 270, 246–266.
Halla, J., Whitehouse, M.J., Ahmad, T., Bagai, Z., 2017. Archaean granitoids: an overview and significance from a tectonic perspective. Geol. Soc. Lond., Spec. Publ. 449 (1), 1–18.
Han, Q.S., Peng, S.B., Kusky, T., Polat, A., Jiang, X., Cen, Y., Lin, S.F., 2017. A Paleoproterozoic ophiolitic mélange, Yangtze craton, South China: Evidence for Paleoproterozoic suturing and microcontinent amalgamation. Precambrian Res. 293, 13–38.
Harnois, L., 1988. The CIW index: a new chemical index of weathering. Sediment. Geol. 55, 319–322.
Hawkesworth, C.J., Dhuime, B., Pietranik, A.B., Cawood, P.A., Kemp, A.I.S., Storey, C.D., 2010. The generation and evolution of the continental crust. J. Geol. Soc. 167 (2), 229–248.
He, H.L., Li, B., Han, L.R., Sun, D.Z., Wang, S.X., Li, S., 2002. Evaluation of determining 47 elements in geological samples by pressurized acid digestion-ICPMS. Chin. J. Anal. Lab. 21, 8–12 (in Chinese with English Abstract).
Herron, M.M., 1988. Geochemical classification of terrigenous sands and shales from core or log data. J. Sediment. Res. 58, 820–829.
Hou, K.J., Li, Y.H., Zhou, T.R., Qu, X.M., Shi, Y.R., Xie, G.Q., 2007. Laser ablation-MC-ICP-MS technique for Hf isotope microanalysis of zircon and its geological applications. Acta Petrol. Sin. 23, 2595–2604.
Hou, K.J., Li, Y.H., Tian, Y.Y., 2009. In situ U-Pb zircon dating using laser ablation-multi ion counting-ICP-MS. Mineral Deposits 28 (4), 481–492 (in Chinese with English abstract).
Hu, J., Liu, X.C., Chen, L.Y., Qu, W., Li, H.K., Geng, J.Z., 2013. A 2.5Ga magmatic event at the northern margin of the Yangtze craton: evidence from U-Pb dating and Hf isotope analysis of zircons from the Douling Complex in the south Qinling orogen. Chin. Sci. Bull. 58, 3564–3579.
Hubei Province Institute of Geologic Survey (HIGS), 1965. 1:200,000 Regional Geological Survey of Yicheng County Hubei Province (in Chinese).
Hubei Province Institute of Geologic Survey (HIGS), 2001. 1:50,000 Regional Geological Survey of Shuanghekou Hubei Province (in Chinese).
Hui, B., Dong, Y.P., Cheng, C., Long, X.P., Liu, X.M., Yang, Z., Sun, S.S., Zhang, F.F., Varga, J., 2017. Zircon U-Pb chronology, Hf isotope analysis and whole-rock geochemistry for the Neoarchean-Paleoproterozoic Yudongzi complex, northwestern margin of the Yangtze craton, China. Precambrian Res. 301, 65–85.
Jackson, S.E., Pearson, N.J., Griffin, W.L., Belousova, E.A., 2004. The application of laser ablation-inductively coupled plasma-mass spectrometry to in situ U-Pb zircon geochronology. Chem. Geol. 211, 47–69.
Jiao, W.F., Wu, Y.B., Yang, S.H., Peng, M., Wang, J., 2009. The oldest basement rock in the Yangtze Craton revealed by zircon U-Pb age and Hf isotope composition. Sci. China Ser. D Earth Sci. 52, 1393–1399.
Johnson, T.E., Brown, M., Gardiner, N.J., Kirkland, C.L., Smithies, R.H., 2017. Earth's first stable continents did not form by subduction. Nature 543, 239–242.
Lan, C.Y., Chung, S.L., Lo, C.H., Lee, T.Y., Wang, P.L., Li, H., Van Toan, D., 2001. First evidence for Archean continental crust in northern Vietnam and its implications for crustal and tectonic evolution in Southeast Asia. Geology 29, 219–222.
Li, Z.X., Zhang, L., Powell, C.M., 1995. South China in Rodinia: part of the missing link between Australia-EastAntarctica and Laurentia? Geology 23, 407–410.
Li, Z.X., Li, X.H., Zhou, H., Kinny, P.D., 2002. Grenvillian continental collision in south China: new SHRIMPU-Pb zircon results and implications for the configuration of Rodinia. Geology 30 (2), 163–166.
Li, Z.X., Li, X.H., Wartho, J.A., Clark, C., Li, W.X., Zhang, C.L., Bao, C., 2010. Magmatic and metamorphic events during the early Paleozoic Wuyi-Yunkai orogeny, southeastern South China: new age constraints and pressure-temperature conditions. Geol. Soc. Am. Bull. 122 (5–6), 772–793.
Li, L.M., Lin, S.F., Davis, D.W., Xiao, W.J., Xing, G.F., Yin, C.Q., 2014. Geochronology and geochemistry of magmatic rocks from the Kongling terrane: implications for Mesoarchean to Paleoproterozoic crustal evolution of the Yangtze Block. Precambrian Res. 255, 30–47.
Li, Y.H., Zheng, J.P., Xiong, Q., Wang, W., Ping, X.Q., Li, X.Y., Tang, H.Y., 2016. Petrogenesis and tectonic implications of Paleoproterozoic metapelitic rocks in the Archean Kongling complex from the northern Yangtze Craton, south China. Precambrian Res. 276, 158–177.
Li, J.H., Zhang, Y.Q., Zhao, G.C., Johnston, S.T., Dong, S.W., Koppers, A., Miggins, D.P., Sun, H.S., Wang, W.B., Xin, Y.J., 2017. New insights into Phanerozoic tectonics of South China: early Paleozoic sinistral and Triassic dextral transpression in the east Wuyishan and Chencai domains, NE Cathaysia. Tectonics 36 (5), 819–853.
Liu, Y.S., Hu, Z.C., Gao, S., Günther, D., Xu, J., Gao, C.G., Chen, H.H., 2008. In situ analysis of major and trace elements of anhydrous minerals by LA-ICP-MS without applying an internal standard. Chem. Geol. 257, 34–43.
Liu, Y.S., Gao, S., Hu, Z.C., Gao, C.G., Zong, K.D., Wang, D.B., 2010. Continental and oceanic crust recycling-inducedmelt-peridotite interactions in the trans-North China Orogen: U-Pb dating, Hf isotopes and trace elements in zircons from mantle xenoliths. J. Petrol. 51, 537–571.
Ludwig, K.R., 2003. User's Manual for Isoplot 3.00: A Geochronological Toolkit for Microsoft Excel, 4. Berkeley Geochronological Center Special Publication, p. 71.
Martin, H., Moyen, J.F., Guitreau, M., Blichert-Toft, J., Le Pennac, J.C., 2014. Why Archean TTGs cannot be generated by melting of MORB melting in subduction zone. Lithos 198–199, 1–13.
McLennan, S.M., 1989. Rare earth elements in sedimentary rocks: influence of provenance and sedimentary processes. Rev. Mineral. Geochem. 21, 169–200.
McLennan, S.M., Taylor, S.R., 1991. Sedimentary rocks and crustal evolution: tectonic setting and secular trends. J. Geol. 99 (1), 1–21.
McLennan, S.M., Hemming, S., McDaniel, D.K., Hanson, G.N., 1993. Geochemical approaches to sedimentation, provenance and tectonics. In: Johnsson, M.J., Basu, A. (Eds.), Processes Controlling the Composition of Clastic Sediments. Vol. 284, pp. 21–40 Geological Society of America, Special Paper.
Nagel, T.J., Hoffmann, J.E., Munker, C., 2012. Generation of Eoarchean tonalite-trondhemite-granodiorite series from thickened mafic crust. Geology 40, 375–378.
Nam, T.N., Toriumi, M., Sano, Y., Terada, K., Thang, T.T., 2003. 2.9, 2.36, and 1.96Ga zircons in orthogneiss south of the Red River shear zone in Viet Nam: evidence from SHRIMPU-Pb dating and tectonothermal implications. J. Asian Earth Sci. 21, 743–753.
Nelson, D.R., 2001. An assessment of the determination of depositional ages for Precambrian clastic sedimentary rocks by U-Pb dating of detrital zircons. Sediment. Geol. 141, 37–60.
Nesbitt, H.W., Young, G.M., 1982. Early Proterozoic climates and plate motions inferred from major element chemistry of lutites. Nature 299, 715–717.
Nesbitt, H.W., Young, G.M., 1989. Formation and diagenesis of weathering profiles. J. Geol. 97, 129–147.
Nie, H., Yao, J., Wan, X., Zhu, X.Y., Siebel, W., Chen, F.K., 2016. Precambrian tectonothermal evolution of south Qinling and its affinity to the Yangtze Block: evidence from zircon ages and Hf-Nd isotopic compositions of basement rocks. Precambrian Res. 286, 167–179.
Nowell, G.M., Kempton, P.D., Noble, S.R., Fitton, J.G., Saunders, A.D., Mahoney, J.J., Taylor, R.N., 1998. High precision Hf isotope measurements of MORB and OIB by thermal ionisation mass spectrometry: insights into the depleted mantle. Chem. Geol. 149 (3), 211–233.
Partin, C.A., Bekker, A., Planavsky, N.J., Scott, C.T., Gill, B.C., Li, C., Podkovyrov, V., Maslov, A., Konhauser, K.O., Lalonde, S.V., Love, G.D., Poulton, S.W., Lyons, T.W., 2013. Large-scale fluctuations in Precambrian atmospheric and oceanic oxygen levels from the record of U in shales. Earth Planet. Sci. Lett. 369–370, 284–293.
Polat, A., 2012. Growth of Archean continental crust in oceanic island arcs. Geology 40, 383–384.

Qin, K.L., Song, S.G., He, S.P., 1992. The geological characteristics of the Yudongzi granite-greenstone terrain and its gold-bearing property in Mianluening area, Shanxi. Northw. Geosci. 13, 65–74 (in Chinese with English abstract).
Qiu, Y.M., Gao, S., McNaughton, N.J., Groves, D.I., Ling, W.L., 2000. First evidence of >3.2Ga continental crust in the Yangtze craton of South China and its implications for Archean crustal evolution and Phanerozoic tectonics. Geology 28, 11–14.
Rudnick, R., Gao, S., 2003. Composition of the continental crust. Treatise Geochem. 3, 1–64.
Rudnick, R., Presper, T., 1990. Geochemistry of intermediate- to high-pressure granulites. In: Vilzeuf, D., Vidal, P. (Eds.), Granulites and Crustal Evolution. Springer, Dordrecht, pp. 523–550.
Scherer, E., Münker, C., Mezger, K., 2001. Calibration of the lutetium-hafnium clock. Science 293.
Shaw, D.M., 1972. The origin of the Apslcy gneiss, Ontario. Can. J. Earth Sci. 9, 18–35.
Sun, M., Chen, N.S., Zhao, G.C., Wilde, S.A., Ye, K., Guo, J.H., Chen, Y., Yuan, C., 2008. U-Pb zircon and Sm-Nd isotopic study of the Huangtuling granulite, Dabie-Sulu belt, China: implication for the Paleoproterozoic tectonic history of the Yangtze craton. Am. J. Sci. 308 (4), 469–483.
Taylor, S.R., McLennan, S.M., 1985. The Continental Crust: Its Composition and Evolution. Blackwell, Oxford, p. 312.
Taylor, S.R., McLennan, M.S., 1995. The geochemical evolution of the continental crust. Rev. Geophys. 33, 293–301.
Taylor, S.R., Rudnick, R., McLennan, S.M., Eriksson, K.A., 1986. Rare earth element patterns in Archean high-grade metasediments and their tectonic significance. Geochim. Cosmochim. Acta 50, 2267–2279.
Tu, Y.J., Yang, X.Y., Zheng, Y.F., Li, H.M., 2001. U-Pb dating of zircon from gneiss at Nanhuang in east Anhui. Acta Petrol. Sin. 17 (1), 157–160 (in Chinese with English abstract).
Wang, W., Zhou, M.F., 2013. Petrological and geochemical constraints on provenance, paleoweathering, and tectonic setting of the Neoproterozoic sedimentary basin in the eastern Jiangnan orogen, south China. J. Sediment. Res. 83 (11), 975–994.
Wang, W., Zhou, M.F., 2014. Provenance and tectonic setting of the Paleo- to Mesoproterozoic Dongchuan Group in the southwestern Yangtze Block, south China: implication for the breakup of the supercontinent Columbia. Tectonophysics 610, 110–127.
Wang, H.L., Xu, X.Y., Chen, J.L., Yan, Z., Li, T., Zhu, T., 2011. Constraint from zircon U-Pb chronology of Yudongzi group magnetite-quartzite in Lueyang area, southern Qinling, China. Acta Geol. Sin. 85 (8), 1284–1290 (in Chinese with English abstract).
Wang, W., Zhou, M.F., Yan, D.P., Li, J.W., 2012a. Depositional age, provenance, and tectonic setting of the Neoproterozoic Sibao Group, southeastern Yangtze Block, south China. Precambrian Res. 192, 107–124.
Wang, X.C., Li, X.H., Li, Z.X., Li, Q.L., Tang, G.Q., Gao, Y.Y., Zhang, Q.R., Liu, Y., 2012b. Episodic Precambrian crust growth: evidence from U-Pb ages and Hf-O isotopes of zircon in the Nanhua Basin, central South China. Precambrian Res. 222, 386–403.
Wang, Z.J., Wang, J., Du, Q.D., Deng, Q., Yang, F., 2013a. The evolution of the Central Yangtze Block during early Neoarchean time: evidence from geochronology and geochemistry. J. Asian Earth Sci. 77, 31–44.
Wang, Z.J., Wang, J., Du, Q.D., Deng, Q., Yang, F., Wu, H., 2013b. Mature Archean continental crust in the Yangtze craton: evidence from petrology, geochronology and geochemistry. Chin. Sci. Bull. 58, 2360–2369.
Wang, W., Zhou, M.F., Zhao, X.F., Chen, W.T., Yan, D.P., 2014. Late Paleoproterozoic to Mesoproterozoic rift successions in SWChina: implication for the Yangtze Block–NorthAustralia–northwest Laurentia connection in the Columbia supercontinent. Sediment. Geol. 309, 33–47.
Wang, Z.J., Wang, J., Deng, Q., Du, Q.D., Zhou, X.L., Yang, F., Liu, H., 2015. Paleoproterozoic I-type granites and their implications for the Yangtze block position in the Columbia supercontinent: evidence from the Lengshui complex, South China. Precambrian Res. 263, 157–173.
Wang, C.L., Huang, H., Tong, X.X., Zheng, M.T., Peng, Z.D., Nan, J.B., Zhang, L.C., Zhai, M.G., 2016a. Changing provenance of late Neoarchean metasedimentary rocks in the Anshan-Benxi area, North China Craton: implications for the tectonic setting of the world-class Dataigou banded iron formation. Gondwana Res. 40, 107–123.
Wang, W., Cawood, P.A., Zhou, M.F., Zhao, J.H., 2016b. Paleoproterozoic magmatic and metamorphic events link Yangtze to northwest Laurentia in the Nuna supercontinent. Earth Planet. Sci. Lett. 433, 269–279.
Wang, X., Zhu, W.B., Liu, Y.Z., Luo, M., Ge, R.F., Zhang, H., Ren, X.M., Cui, X., 2017. Revisiting the Yejishan Group of the Lüliang Complex, North China: implications for a Paleoproterozoic active continental marginal basin in the trans-North China Orogen. Precambrian Res. 292, 93–114.
Wang, K., Li, Z.X., Dong, S.W., Cui, J.J., Han, B.F., Zheng, T., Xu, Y.L., 2018. Early crustal evolution of the Yangtze craton, South China: new constraints from zircon U-Pb-Hf isotopes and geochemistry of ca. 2.9–2.6Ga granitic rocks in the Zhongxiang Complex. Precambrian Res. 314, 325–352.
White, A.F., Blum, A.E., 1995. Effects of climate on chemical weathering in watersheds. Geochim. Cosmochim. Acta 59 (9), 1729–1747.
Winkler, H.G.F., 1976. Petrogenesis of Metamorphic Rocks. 2nd ed. Springer-Vedag, New York, p. 237.
Wu, Y.B., Gao, S., Gong, H.J., Xiang, H., Jiao, W.F., Yang, S.H., Liu, Y.S., 2009. Zircon U-Pb age, trace element and Hf isotope composition of Kongling terrane in the Yangtze Craton: refining the timing of Palaeoproterozoic high-grade metamorphism. J. Metamorph. Geol. 27, 461–477.
Wu, Y.B., Gao, S., Zhang, H., Zheng, J.P., Liu, X., Wang, H., Gong, H., Zhou, L., Yuan, H., 2012. Geochemistry and zircon U-Pb geochronology of Paleoproterozoic arc related granitoid in the Northwestern Yangtze Block and its geological implications. Precambrian Res. 2009, 26–37.
Wu, Y.B., Zheng, Y.F., Gao, S., Jiao, W.F., Liu, Y.S., 2008. Zircon U-Pb age and trace element evidence for Paleoproterozoic granulite-facies metamorphism and Archean crustal rocks in the Dabie Orogen. Lithos 101, 308–322.
Wu, Y.B., Zhou, G.Y., Gao, S., Liu, X.C., Qin, Z.W., Wang, H., Yang, J.Z., Yang, S.H., 2014. Petrogenesis of Neoarchean TTG rocks in the Yangtze Craton and its implication for the formation of Archean TTGs. Precambrian Res. 254, 73–86.
Yang, J.H., Cawood, P.A., Du, Y.S., Li, W.Q., Yan, J.X., 2016. Reconstructing early Permian tropical climates from chemical weathering indices. Geol. Soc. Am. Bull. 128 (5–6), 739–751.
Yin, C.Q., Lin, S.F., Davis, D.W., Zhao, G.C., Xiao, W.J., Li, L.M., He, Y.H., 2013. 2.1–1.85Ga tectonic events in the Yangtze Block, south China: Petrological and geochronological evidence from the Kongling Complex and implications for the reconstruction of supercontinent Nuna. Lithos 182–183 (12), 200–210.
Young, G.M., 1999. Some aspects of the geochemistry, provenance and palaeoclimatology of the Torridonian of NW Scotland. J. Geol. Soc. Lond. 156, 1097–1111.
Zhang, S.B., Zheng, Y.F., 2013. Formation and evolution of Precambrian continental lithosphere in South China. Gondwana Res. 23, 1241–1260.
Zhang, Z.Q., Zhang, G.W., Tang, S.H., Wang, J.H., 2001. On the age of metamorphic rocks of the Yudongzi Group and the Archean crystalline basement of the Qingling Orogen. Acta Geol. Sin. 75, 198–204 (in Chinese with English abstract).
Zhang, S.B., Zheng, Y.F., Wu, Y.B., Zhao, Z.F., Gao, S., Wu, F.Y., 2006. Zircon isotope evidence for ≥3.5Ga continental crust in the Yangtze craton of China. Precambrian Res. 146, 16–34.
Zhang, X., Xu, X.Y., Song, G.S., Wang, H.L., Chen, J.L., Li, T., 2010. Zircon LA-ICP-MSU-Pb dating and significance of Yudongzi Group deformation granite from Lueyang area, western Qinling, China. Geol. Bull. China 29, 510–517 (in Chinese with English abstract).
Zhang, L.J., Ma, C.Q., Wang, L.X., She, Z.B., Wang, S.M., 2011. Discovery of Paleoproterozoic rapakivi granite on the northern margin of the Yangtze block and its geological significance. Chin. Sci. Bull. 1 (3), 306–318.
Zhao, G.C., Cawood, P.A., 2012. Precambrian geology of China. Precambrian Res. 222–223, 13–54.
Zhao, X.F., Zhou, M.F., 2011. Fe-cu deposits in the Kangdian region, SWChina: a Proterozoic IOCG (iron-oxide-copper-gold) Metallogenic Province. Mineral. Deposita 46 (7), 731–747.
Zhao, G.C., Cawood, P.A., Wilde, S.A., Sun, M., 2002. Review of Global 2.1–1.8Ga Orogens: implications for a pre-Rodinia supercontinent. Earth Sci. Rev. 59, 125–162.
Zhao, X.F., Zhou, M.F., Li, J.W., Sun, M., Gao, J.F., Sun, W.H., Yang, J.H., 2010. Late Paleoproterozoic to early Mesoproterozoic Dongchuan Group in Yunnan, SWChina: implications for tectonic evolution of the Yangtze Block. Precambrian Res. 182 (1), 57–69.
Zhou, B.G., Wang, S.W., Sun, X.M., Liao, Z.W., Guo, Y., Jiang, X.F., Zhu, H.P., Liu, C.Z., Luo, M.J., Ma, D., Shen, Z.W., Zhang, H., 2012. SHRIMP U-Pb age and its significance of zircons in welded tuff of Wangchang formation in Dongchuan area, Yunnan Province, SWChina. Geol. Rev. 58 (2), 359–368 (in Chinese with English abstract).
Zhou, G.Y., Wu, Y.B., Gao, S., Yang, J.Z., Zheng, J.P., Qin, Z.W., Wang, H., Yang, S.H., 2015. The 2.65Ga A-type granite in the northeastern Yangtze craton: Petrogenesis and geological implications. Precambrian Res. 258, 247–259.
Zhou, G.Y., Wu, Y.B., Wang, H., Qin, Z.W., Zhang, W.X., Zheng, J.P., Yang, S.H., 2017. Petrogenesis of the Huashanguan A-type granite complex and its implications for the early evolution of the Yangtze Block. Precambrian Res. 292, 57–74.
Zhu, H.P., Fan, W.Y., Zhou, B.G., Wang, S.W., Luo, M.J., Liao, Z.W., Guo, Y., 2011. Assessing Precambrian stratigraphic sequence of Dongchuan area: evidence from zircon SHRIMP and LA-ICP-MS dating. Geol. J. China Univ. 17 (3), 452–461 (in Chinese with English abstract).